ACS Catalysis

pubs.acs.org/acscatalysis

Research Article

Catalytic Consequences of Oxidant, Alkene, and Pore Structures on Alkene Epoxidations within Titanium Silicates

Daniel T. Bregante, Jun Zhi Tan, Rebecca L. Schultz, E. Zeynep Ayla, David S. Potts, Chris Torres, and David W. Flaherty*

Cite This: *ACS Catal.* 2020, 10, 10169−10184

Read Online

ACCESS | Metrics & More | Article Recommendations | Supporting Information

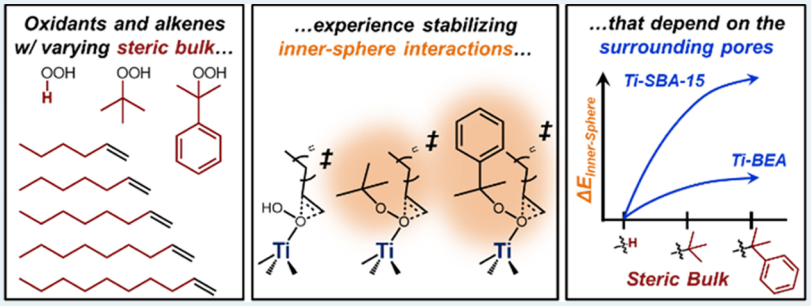

ABSTRACT: Ti atoms incorporated into the framework of zeolite *BEA (Ti-BEA) or grafted onto SBA-15 (Ti-SBA-15) catalyze alkene epoxidation with hydrogen peroxide (H_2O_2), *t*-butyl hydrogen peroxide (TBHP), or cumene hydroperoxide (CHP). The rates of epoxidation, however, differ by orders of magnitude depending on the combination of an oxidant, an alkene, and a support used. Within Ti-BEA, the rates of 1-octene epoxidation with H_2O_2 are 30 and 170 times greater than reactions with TBHP or CHP, respectively. In contrast, 1-octene epoxidation rates in Ti-SBA-15 with H_2O_2 are 7- and 40-fold higher than in reactions with TBHP or CHP, respectively. Moreover, comparisons of 1-alkene (C_6−C_{10}) epoxidations within Ti-BEA and Ti-SBA-15 show that the turnover rates depend differently on the length of alkene reactants depending on the oxidant identity, which is due to complex interactions among the alkene, the activated oxidant, and the solvent-filled pore of the Ti-silicate. Thermochemical analyses of apparent activation free energies within a Born−Haber cycle reveal three distinct contributions that affect catalysis, which include charge transfer between Ti-OOR and C═C functions within the transition state; the adsorption of the alkene into the silicate pores; and the structural rearrangement of the reactive Ti-OOR intermediates and solvent to accommodate the alkene. First, epoxidations with H_2O_2 give the highest rates among these oxidants because Ti-OOH intermediates are more electrophilic than Ti-OO*t*Bu or Ti-OOcumyl species as a consequence of electron donation from alkyl groups that increase intrinsic barriers for O-atom transfer. Second, differences in the epoxidation rates between Ti-BEA and Ti-SBA-15 largely reflect the changes in the stability of the alkenes adsorbed within the pores of each silicate. Third, the distinct sensitivities of epoxidation rates on oxidant identity within Ti-BEA and Ti-SBA-15 are caused by differences between the inner-sphere interactions among Ti-OOR intermediates and adsorbed alkenes that depend on the surrounding environment. We present a thermodynamic model that quantitatively describes how inner-sphere interactions among epoxidation transition states depend on the steric bulk of the reacting species and how these interactions are conferred by the topology of the surrounding pore. The mesopores of Ti-SBA-15 allow transition states to access conformations that lower the free energy of the complex relative to analogous transition states in Ti-BEA, which explains why epoxidation rates in mesoporous solids are less sensitive to the identity of the oxidant than within microporous silicates.

KEYWORDS: *zeolites, solid−liquid interfaces, inner sphere, steric interactions, oxidations, hydrogen peroxide, tert-butyl hydroperoxide, cumene hydroperoxide*

1. INTRODUCTION

Molecular interactions among surface intermediates during catalysis contribute directly to the free energies of critical reactive species[1−3] and, therefore, impact rates and selectivities. Interactions between reactive complexes with functions outside of the first-coordination sphere (e.g., solvents and pore walls) are colloquially referred to as outer-sphere interactions, whereas interactions among species directly bound to an active site (e.g.,

Received: May 17, 2020
Revised: August 10, 2020
Published: August 12, 2020

https://dx.doi.org/10.1021/acscatal.0c02183
ACS Catal. 2020, 10, 10169−10184

among ligands and charge transfer) are known as inner-sphere interactions.[4,5] Organometallic chemists commonly consider both inner- and outer-sphere interactions to design complex ligands that facilitate reactions at molecular complexes;[6,7] yet, the heterogeneous catalysis community less frequently invokes these principles to design solid surfaces for desired chemical transformations. This is due, in part, to the structural complexities of surfaces, pores, and confined solvents that surround active sites and reactive intermediates.[1,8,9]

The conformation and stability of surface species bound to active sites depend on the presence and topology of surrounding pores,[10−13] which consequently influence the rates of reactions along specific pathways. Comparisons of catalysis within zeolites (e.g., MFI, *BEA, and FAU) and in mesoporous silicas (e.g., SBA-15[14,15] and MCM-41[16,17]) provide a convenient method to understand how molecular interactions and reactive species conformation depend on pore structure and functionality (e.g., hydrophilicity) because these classes of materials possess well-defined pore topologies that extend over the relevant range of distances (i.e., 0.5−>5 nm). Silicates that contain early transition metal atoms (e.g., Ti,[18−26] Nb,[4,18,24,27,28] and Ta[18,29,30]) activate hydroperoxide oxidants and catalyze alkene epoxidations that involve transition states composed of reactive metal-peroxides, hydroperoxides, alkyl peroxides, or oxo intermediates and alkenes in solvent-filled pores. Consequently, the stabilities of reactive species and transition states for alkene epoxidation should sense changes in the steric bulk of the substituent groups on the hydroperoxides and alkene reactants, the impact of these substituents on the electronic structure of the reactive intermediates, and the spatial constraints introduced by the catalyst pores.

For decades, researchers sought to explain how rates of alkene epoxidation depend on the structure of the alkene reactants and the (alkyl) hydroperoxide oxidants and why specific combinations of titanosilicates, oxidants, alkenes, and solvents perform better than others.[5,23−26,31−36] Multiple industrial processes currently produce propylene oxide by direct propylene epoxidation with either hydrogen peroxide (H_2O_2; hydrogen peroxide-propylene oxide process[34,37]), *t*-butyl hydrogen peroxide (TBHP; e.g., Halcon and ARCO processes[38−40]), cumene hydroperoxide (CHP; e.g., propylene oxide-only process[41]), or ethylbenzene hydroperoxide (e.g., Shell styrene monomer-propylene oxide process[39]). Seminal studies[24,25,42] on epoxidation within Ti-silicates have reported on changes in the yields and selectivities toward epoxide products with different combinations of oxidants, solvents, and catalysts. The reported differences between the unique combinations of the oxidant, solvent, and catalyst likely reflect intramolecular interactions among the reactive intermediates, adsorbed alkenes, and solvent-filled pores, whose quantification is a challenge in the catalysis community.

Tatsumi and co-workers showed that the conversion of cyclohexene, cycloheptene, and cyclododecene in epoxidations are on average fivefold greater with H_2O_2 than with TBHP within Ti-BEA (∼ 1.6 M alkene, 0.5 M H_2O_2, CH_3OH solvent, 333 K, 3 h),[42] and the authors attributed the differences in rates to repulsive interactions between the bulky *t*-butyl group of Ti-OO*t*Bu intermediates and the alkene reagents. Similarly, rates of cyclohexene epoxidation with H_2O_2 are 20% greater than with TBHP over Ti-substituted MCM-41 materials;[43] however, the reasons for the observed differences in rates were not discussed. Within the mesoporous Ti-MFI material, 1-octene epoxidation rates are 6-times higher with TBHP than with H_2O_2,[44] which was associated with the presence of hydrophilic silanol functions within the mesopores inhibiting H_2O_2 activation and the greater rates of intrapore diffusion of TBHP to access active sites and react. These prior reports may also reflect the convoluting effects of intraparticle mass transfer restrictions that obfuscate the impact of pore confinement, alkene conformation, and inner-sphere interactions on chemical kinetics. As such, a quantitative molecular understanding of how the combination of alkenes, oxidants, and pore diameters leads to changes in the stability of surface intermediates and epoxidation rates remains elusive.

Here, we assess how the stabilities of epoxidation transition states depend on the identity of the Ti-OOR intermediates, the steric bulk of the 1-alkenes, and the size of the surrounding pores through the thermochemical analysis of reaction kinetics. We measure turnover rates, activation barriers, and alkene adsorption enthalpies on catalysts composed of Ti atoms within the framework of *BEA (Ti-BEA) and Ti atoms grafted to mesoporous SBA-15 (Ti-SBA-15) and establish quantitative relationships that describe how interactions among oxidants and alkenes depend on the morphological properties of the catalyst. For both catalysts, the turnover rates for 1-octene epoxidation are greatest with H_2O_2, in comparison with TBHP and CHP, yet, vary by up to 40- or 170-fold within Ti-SBA-15 and Ti-BEA, respectively. Moreover, the rates of 1-octene epoxidation within Ti-BEA are 10−100 times greater than within Ti-SBA-15, for any given oxidant. The strong dependence of epoxidation rates on the combination of the oxidant and pore diameter does not reflect differences in the mechanism for epoxidation, which are equivalent among all combinations of the alkene, oxidant, and catalyst tested. Instead, the differences in turnover rates reflect free-energy contributions from the charge transfer between Ti-OOR intermediates and the C═C to form the transition state, the adsorption of the alkene into the silicate pores, and the restructuring of the reactive Ti-OOR intermediates and solvent molecules to accommodate the alkene. Thermochemical analysis of apparent activation free energies within a Born−Haber cycle, in conjunction with Hammett analysis, reveals that Ti-OOH intermediates are more electrophilic than Ti-OO*t*Bu or Ti-OOcumyl species and possess lower intrinsic barriers for O-atom transfer. Differences in the free energies of 1-alkene adsorption into siliceous BEA and SBA-15 correspond to differences in the epoxidation rates for reactions with H_2O_2 and suggest why rates are greater within Ti-BEA than within Ti-SBA-15. The ways in which epoxidation rates depend on oxidant identity within Ti-BEA in comparison with Ti-SBA-15, however, reflect inner-sphere interactions among Ti-OOR intermediates and adsorbed alkenes that derive from the topology of the silicate pores. We present a simple thermodynamic model that quantitatively describes how inner-sphere interactions among two reacting species that are nominally bound to an active site change with the steric bulk of the reacting species. Analysis of apparent activation free energies (and epoxidation rates) within this framework reveals that the mesopores of Ti-SBA-15 allow for specific inner-sphere interactions among Ti-OOR intermediates and 1-alkenes that lower the free energy of the transition states relative to the micropores of Ti-BEA. These stabilizing interactions, however, do not entirely compensate for the differences in 1-alkene adsorption into the micropores of BEA relative to SBA-15; rather, they result in distinct dependencies of turnover rates on the combination of alkenes, oxidants, and pore structures.

Collectively, the findings presented here provide molecular insight into the free-energy contributions and molecular

https://dx.doi.org/10.1021/acscatal.0c02183
ACS Catal. 2020, 10, 10169−10184

interactions that elucidate how the selection of hydroperoxide oxidants, alkene substrates, and Ti-silicate topology impact epoxidation rates and begin to explain the reasons for singular combinations of reactants, solvents, and catalysts for industrial propylene epoxidation processes.

2. MATERIALS AND METHODS

2.1. Catalyst Synthesis. Ti-BEA-12.5, where "12.5" refers to the initial Si/Al ratio of the parent Al-BEA-12.5 (Zeolyst, CP814E; Si/Al ~ 12.5; surface area ~ 680 $m^2 g^{-1}$), was prepared by postsynthetic modification. Al-BEA-12.5 was refluxed in HNO_3 (Macron Chemicals, 68−70 wt %; 20 $cm^3 g_{Al\text{-}BEA}^{-1}$; *caution: HNO_3 is a strong oxidant, readily causes a chemical burn, and should be handled carefully*) with the intent to remove framework Al atoms by forming soluble $Al(NO_3)_3$. The solids were then recovered by vacuum filtration and washed with H_2O (17.8 MΩ · cm, 50 $cm^3 g^{-1}$) followed by heating at 5 K min^{-1} in flowing air (100 $cm^3 min^{-1}$; Airgas, Ultra-zero grade) and held at 823 K for 6 h to remove residual volatile and organic species and to produce Si-BEA-12.5. The materials produced in this manner possessed Si/Al ratios greater than 1400, as determined by energy dispersive X-ray fluorescence spectroscopy. Ti atoms were incorporated by combining a stirred suspension of Si-BEA-12.5 with an appropriate amount of $TiCl_4$ (Sigma-Aldrich, 99.9%) in CH_2Cl_2 (Fisher Chemicals, Certified ACS Stabilized) at reflux. *Caution: $TiCl_4$ reacts violently with moisture in air to form HCl and should be handled carefully*. All volatile components were then removed by rotary evaporation. The recovered solids were light brown, and these materials were heated in flowing air (100 $cm^3 min^{-1}$) at 5 K min^{-1} to 823 K and held at that temperature for 6 h, which produced bright white solid powders.

Ti-BEA-F was synthesized hydrothermally in fluoride media by adapting a previously published procedure.[3,45] Tetraethylammonium fluoride (TEAF, Alfa Aesar, 97 wt %) was dissolved in deionized H_2O (18.2 MΩ · cm) in a polypropylene container and combined with titanium(IV) isopropoxide (TIPO, Sigma-Aldrich, 99.999%) to produce a clear homogeneous solution. Tetraethylorthosilicate (TEOS, Sigma-Aldrich, >98 wt %) was then added slowly over a period of 1 min to this solution under static conditions, which initially formed a biphasic mixture. The mixture was then stirred for 16 h to produce an opaque homogeneous solution. The lid of the polypropylene container was then removed to evaporate the ethanol and isopropanol that form through the hydrolysis of the TEOS and TIPO, respectively. The solution was left open while stirring until the mass of the solution decreased by 115% of the value of the estimated mass of the alcohols to ensure that the alcohols evaporated completely. Subsequently, deionized H_2O was added to yield a gel with a final molar composition of 1 SiO_2/0.0033 TIPO/0.56 TEAF/7 H_2O. *Note: this synthesis procedure produces MFI when crystallized if the ethanol and isopropanol are not entirely evaporated.* This gel was then loaded into a Teflon-lined stainless-steel autoclave (Parr Instruments, 45 cm^3) that contained 5 wt % (relative to SiO_2 within the gel) Si-BEA-12.5 as seeds to promote the formation of the BEA zeolite. This autoclave was then sealed and heated to 413 K while rotating (60 rpm) in a convection oven (Yamato, DKN602C) for 25 days. The resulting solids were recovered, washed with H_2O, and dried for 16 h at 373 K. The dried solids were then heated at 1 K min^{-1} to 823 K in flowing air (100 $cm^3 min^{-1}$) and held at 823 K for 10 h to produce a bleached-white solid.

Ti-SBA-15 was synthesized by the liquid-phase grafting of titanocene dichloride ($TiCp_2Cl_2$; Sigma-Aldrich, 97%) onto a mesoporous silica (SBA-15; ACS Material, 7−10 nm pores; surface area ~ 450 $m^2 g^{-1}$).[14,15] SBA-15 was heated at 5 K min^{-1} to 823 K in flowing air (100 $cm^3 min^{-1}$) and held at 823 K for 6 h to dehydrate and partially dehydroxylate the surface. The dried SBA-15 was stored within a vacuum desiccator until further use. The dried SBA-15 was then stirred in a solution of $TiCp_2Cl_2$ in CH_2Cl_2 under an argon atmosphere at 298 K using standard Schlenk technique, which yielded a bright-red slurry. The desired amount of triethylamine ($N(Et)_3$; Sigma-Aldrich, 99.5%) was then added (in a 2.5:1 ratio, relative to $TiCp_2Cl_2$) to the slurry, with the intent to deprotonate surface SiOH groups to graft $TiCp_2Cl_2$. This suspension was stirred for 6 h at 298 K, and the suspension slowly turned bright yellow in color over this time period. The solids were then recovered via filtration and were washed with CH_2Cl_2 (20 $cm^3 g^{-1}$). The recovered solids were pale yellow in appearance and were heated at 5 K min^{-1} to 823 K in flowing dry air (100 $cm^3 min^{-1}$) at 823 K for 6 h to remove the cyclopentadienyl ligands and produce a bleached white solid.

2.2. Catalyst Characterization. X-ray diffractograms were collected using a diffractometer (Siemens/Bruker, D5000) with a Cu Kα radiation source (0.15418 nm) under ambient conditions. The X-ray diffractograms (Figure S1) for Ti-BEA-12.5 and Ti-BEA-F match the known diffraction patterns of *BEA.

Table 1. Ti Metal Loadings, Band Edge Energies, and BET-Derived Surface Areas for Ti-BEA and Ti-SBA-15 Materials

sample	Ti content[a] (wt %)	band edge energy[b] (eV)	BET surface area ($m^2 g^{-1}$)[c]
Ti-BEA-12.5	0.20	4.2	610
Ti-BEA-F	0.15	4.3	407
Ti-SBA-15	0.30	4.0	443

[a]Measured by EDRXF. [b]Determined from the leading edge of the Tauc plot from DRUV−vis. [c]Calculated from N_2 adsorption isotherms.

Band edge energies (Table 1) were measured by diffuse reflectance UV−vis spectroscopy (DRUV−vis). In short, the samples were intimately ground with magnesium oxide (MgO; Sigma-Aldrich, 99.995%) in a 1:10 ratio of Ti-silicate to MgO by mass. These samples were loaded into a Harrick diffuse-reflectance accessory, and spectra were obtained using a spectrophotometer (Agilent, CARY5) with pure MgO as the background. All materials possess a single UV−vis absorbance feature around 260 nm (Figure S2), which is qualitatively consistent with hydrated isolated Ti^{4+} ions. Band edges calculated from the corresponding Tauc plots (Table 1) are significantly greater than bulk TiO_2 (~ 3.2 eV),[18] which suggests that all Ti-silicates within this study contain highly disperse Ti atoms and possess few, if any, larger TiO_x aggregates.

Metal contents were quantified using energy-dispersive X-ray fluorescence (EDXRF) spectroscopy. Briefly, ~30 mg of the catalyst was loaded into a polypropylene sample holder (1 cm diameter) that was sealed with ultralene film. The samples were loaded into a spectrometer (Shimadzu, EDX-7000), whose sample chamber was purged with He (Airgas, Ultra-zero grade). Measurements were taken between 0 and 30 keV (100 co-averaged scans), and the relative intensities of the element-specific fluorescence features (Figure S3) were used to calculate the percent, by mass, of each element within the sample.

https://dx.doi.org/10.1021/acscatal.0c02183
ACS Catal. 2020, 10, 10169−10184

Gas-phase adsorption isotherms (Figure S4) were collected on a volumetric adsorption instrument (Micromeritics, 3Flex). The Ti-silicate samples were pelletized and sieved to retain particles greater than 180 μm in diameter. These samples were degassed by heating under vacuum ($<7 \times 10^{-4}$ Pa, 673 K) for 6 h prior to adsorption measurements. N_2 adsorption was conducted at 77 K.

1-Octene (C_8H_{16}) adsorption enthalpies were measured by van't Hoff analysis of the change in C_8H_{16} uptake into Si-BEA-12.5 and SBA-15 as a function of temperature within the linear regime of the adsorption isotherm. A solution of C_8H_{16} in CH_3CN (20 cm^3) was heated to the desired temperature (308−333 K) within a 25 cm^3 reaction vessel and was shaken at 250 rpm. An aliquot of the solid-free solution was taken and analyzed via gas chromatography (GC; HP, 5890) to determine the initial peak areas of C_8H_{16} at a given concentration. The desired amount of BEA-12.5 or SBA-15 (∼ 60 mg) was then added to the reactor, and the system was equilibrated at a given temperature for 1 h. An aliquot was then filtered through a syringe filter (0.22 μm; polypropylene) to remove the solids and was subsequently analyzed via GC. This process was repeated for a series of C_8H_{16} concentrations (1 μM to 1 mM) to determine the region where the amount of adsorbed C_8H_{16} is proportional to the concentration of C_8H_{16} in the equilibrated solution (see Section S1.5). The uptake of C_8H_{16} was then measured as a function of temperature to determine the enthalpies of adsorption of C_8H_{16} into Si-BEA-12.5 and SBA-15, which are calculated as -85 ± 6 and -51 ± 5 kJ mol^{-1}, respectively.

2.3. Measurement of Epoxidation Rates. 1-Hexene (C_6H_{12}; Sigma-Aldrich, >99%), 1-heptene (C_7H_{14}; TCI Chemicals, >98%), 1-octene (C_8H_{16}; Sigma-Aldrich, 98%), 1-nonene (C_9H_{18}, TCI Chemicals, >95%), 1-decene ($C_{10}H_{20}$, TCI Chemicals, >95%), styrene (Sigma-Aldrich, ReagentPlus, >99%), 4-bromostyrene (TCI Chemicals, >95%), H_2O_2 (Fischer Chemicals, 30 wt % in H_2O), *tert*-butyl hydroperoxide (TBHP; Sigma Aldrich, 5.5 M in decane), cumene hydroperoxide (CHP; TCI Chemicals, 80% with aromatic hydrocarbons), decane (TCI Chemicals, >99%), acetonitrile (CH_3CN; Fisher Chemicals, HPLC Grade), copper (II) sulfate ($CuSO_4$; Fisher Chemicals, >98.6%), neocuproine (Sigma-Aldrich, >98%), ethanol (Decon Labs; 100%), and H_2O (18.2 MΩ cm) were used as received.

The rates of alkene epoxidation and oxidant decomposition were measured using batch reactors (100 cm^3, three-neck round-bottom flasks) equipped with reflux condensers to minimize evaporative losses. An alkene and a peroxide oxidant (i.e., H_2O_2, TBHP, or CHP) were added to a solution of CH_3CN and decane (used as an internal standard for GC analysis) and heated to the desired temperature (303−348 K) while stirring at 700 rpm. The reactions were initiated by the addition of a catalyst, and small aliquots (∼ 500 μL) of the reaction solution were extracted through a syringe filter (0.22 μm, polypropylene) at predetermined time intervals. The concentrations of the organic components within these aliquots were quantified via gas chromatography. All species were identified, and calibration factors were quantified using the standards of known concentrations. The concentration of H_2O_2 in each aliquot was measured by colorimetric titration using an aqueous solution of $CuSO_4$ (8.3 mM), neocuproine (12 mM), and ethanol (25% v/v). The concentration of H_2O_2 was calculated by comparison of the absorbance at 454 nm to calibrated standards, measured on a spectrophotometer (Spectronic, 20 Genesys). In all reported data, the standard uncertainty for measured reaction rates was below 10%. For all reactions, only the 1,2-epoxyalkane product was observed, which reflects the intentionally low conversion over which these experiments were conducted (see below). The rates for the conversion of the alkene and oxidant were determined using the method of initial rates and were measured as functions of reactant concentrations. All reported results were obtained at differential conversion (i.e., <0.5% conversion of the limiting reagent); consequently, all reported rates do not reflect artifacts associated with catalyst deactivation. For all combinations of oxidants and Ti-silicates, alkene epoxidation kinetics were measured in the absence of mass-transfer artifacts, as indicated by turnover rates that depend linearly on the concentration of the alkene (Section 3.2).[46]

The percent of active Ti atoms in Ti-SBA-15 was determined by in situ site titrations with *t*-butylphosphonic acid (TBPA; Sigma-Aldrich, 98%) during the epoxidation of C_8H_{16} (0.01 M C_8H_{16}, 0.01 M H_2O_2, 313 K). In short, a suspension containing Ti-BEA (∼ 30 mg), C_8H_{16}, decane (as an internal standard), and TBPA in CH_3CN was stirred for at least 1 h at 313 K with the intent to irreversibly bind TBPA to active sites and inhibit epoxidation catalysis. Then, H_2O_2 was added to the reactor to initiate catalysis. Epoxidation rates were measured for systems with ratios of TBPA/Ti ranging from zero to unity. The percentage of Ti atoms that are active for epoxidation was determined by the linear extrapolation of these data to determine the TBPA/Ti ratio that gives a rate equal to zero (Figure S6) and was found to be 95 ± 4%. We have previously used this methodology to determine the percent of active Ti atoms within these Ti-BEA-12.5 and Ti-BEA-F samples as 102 ± 7 and 92 ± 6%, respectively.[47] For all reported kinetics, the number of *active* Ti atoms, as determined from phosphonic acid site titrations, were used to determine turnover rates.

2.4. In Situ UV−Vis Spectroscopy. UV−vis spectra were collected using a 45° diffuse reflection probe (Avantes, solarization-resistant fibers) coupled to a fiber-optic spectrometer (Avantes, AvaFast 2048) with a compact deuterium−halogen light source (Avantes, AvaLight-DHc). The samples were pressed into 7 mm diameter pellets (∼ 5 mg) and loaded into a liquid flow cell with temperature control. Solutions were introduced using a high-performance liquid chromatography pump (Teledyne SSI, M1). Background UV−vis spectra (average of 100 scans) were obtained for each material by exposing the sample to a flowing CH_3CN solution (39 mM H_2O, 1 cm^3 min^{-1}) at 313 K for 0.5 h. Spectra were obtained while flowing solutions of H_2O_2 or CHP in CH_3CN at 313 K and continued until the UV−vis spectra became constant, which implies that the system reached a steady state. All UV−vis spectra presented represent the difference between the experimental spectra and the background spectra.

3. RESULTS AND DISCUSSION

3.1. Activation of Oxidants at Ti Active Sites. Hydrogen peroxide, *t*-butyl hydroperoxide (TBHP), and cumene hydroperoxide (CHP) react over Ti atoms incorporated into the zeolite framework to form Ti-OOH and Ti-OOR (R = *t*-butyl or cumyl) intermediates. Figure 1 shows that the UV−vis spectra of H_2O_2- and CHP-activated Ti-BEA-12.5 and Ti-SBA-15 possess a broad, asymmetric feature whose peak areas are assumed to be proportional to the surface coverage of each UV−vis active intermediate. The broad features between 300 and 450 nm for H_2O_2-activated Ti-BEA-12.5 (Figure 1a) and Ti-SBA-15

https://dx.doi.org/10.1021/acscatal.0c02183
ACS Catal. 2020, 10, 10169−10184

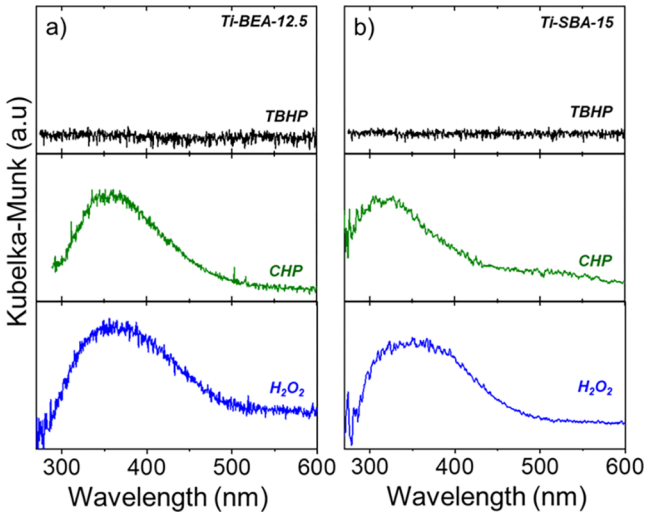

Figure 1. UV−vis difference spectra of H_2O_2- (10 mM H_2O_2, 39 mM H_2O), CHP- (0.3 M CHP, 39 mM H_2O), and TBHP-activated (10 mM TBHP, 39 mM H_2O) (a) Ti-BEA-12.5 and (b) Ti-SBA-15 in CH_3CN at 313 K. In all cases, the background spectra are of the indicated Ti-silicate in CH_3CN (39 mM H_2O) at 313 K.

(Figure 1b) represent overlapping ligand-to-metal charge transfer (LMCT) bands attributed to the Ti-(η^2-O_2) and Ti-OOH intermediates.[20,47−53] Previous work indicates that among this pool of Ti-peroxide intermediates, only Ti-OOH reacts directly with alkenes, as indicated through stereoselective *cis*-stilbene epoxidation and the kinetic modeling of Ti-OOH and Ti-(η^2-O_2) consumption monitored via time-resolved UV−vis spectra.[20,47−53] Therefore, catalytic comparisons (Sections 3.2−3.4) within this study will be between Ti-OOH and Ti-OOR intermediates. Titanium cumyl-peroxide (Ti-OOcumyl) species show an LMCT absorbance between 300 and 450 nm (Figure 1). This complex UV−vis feature does not correspond to fluid-phase CHP or 2-phenyl-2-propanol in the solution because these species possess absorbance features near 260 nm.[54] Ti-OO*t*Bu species have been identified over mesoporous Ti-MCM-41 via X-ray absorption spectroscopy;[35,55,56] however, we were unable to observe features in the UV−vis spectra of TBHP-activated samples (Figure 1). Consequently, we extend the interpretation of CHP activation measurements to TBHP, based on the expectation that titanium alkylperoxides (i.e., Ti-OOcumyl and Ti-OO*t*Bu) will react similarly.

The epoxidation catalysis community does not agree on the kinetic relevance of elementary steps that activate ROOH over Ti-silicates. For example, many studies describe ROOH activation as reversible or quasi-equilibrated (Scheme 1),[18,19,49,57] while other groups have suggested that Ti-OOH forms irreversibly.[47,48,58] Ongoing efforts within our group, including those presented here, show that the kinetics of ROOH activation over early transition metals substituted into zeolites or supported on mesoporous oxides depends on both the identity of the ROOH and the solvent.

Scheme 1. Adsorption and Activation of H_2O_2, CHP, or TBHP To Form Ti-OOR Intermediates[a]

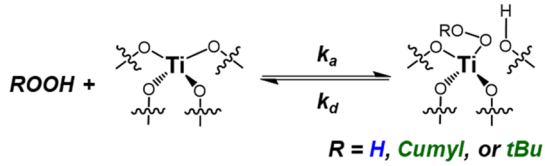

[a] k_a and k_d represent the apparent first-order rate constants for the adsorption and activation or desorption, respectively, of H_2O_2, CHP, or TBHP.

Figure 2 shows the normalized absorbance areas for the LMCT of Ti-OOH and Ti-OOcumyl species present on Ti-BEA-12.5 as a function of time in flowing CH_3CN (39 mM H_2O, 1 cm^3 min^{-1}, 313 K). The coverages of Ti-OOR intermediates were first established by contact with CH_3CN solutions containing either H_2O_2 (10 mM) or CHP (0.3 M) at 313 K until reaching the steady state, after which an oxidant-free solution was introduced to determine whether ROOH species activate reversibly (as depicted in Scheme 1). The number of Ti-OOH species does not change when H_2O_2-activated Ti-silicates (Figure 2 and Figure S8) contact CH_3CN, which suggests that Ti-OOH intermediates form irreversibly within CH_3CN (i.e., the value of k_d for Ti-OOH is immeasurably small). Ti-OOcumyl species, however, recombinatively desorb following pseudo-first-order kinetics (Figure 2 and Figure S8), thus form reversibly over Ti active sites. The rate constants for the desorption (i.e., values of k_d) of CHP from Ti-OOcumyl intermediates from Ti-BEA-12.5 and Ti-SBA-15 (Section S2) are 2.8×10^{-3} and 3.3×10^{-2} s^{-1}, respectively. Collectively, these data and interpretations show that alkyl hydroperoxides activate reversibly and H_2O_2 activates irreversibly in CH_3CN to form Ti-OOR intermediates. Ti-OOH intermediates are in an acid−base equilibrium with Ti-(η^2-O_2);[48,50,59−61] existing studies on the H_2O_2 activation of Ti^{4+} metal centers in polyoxometallates suggest that Ti-(η^2-O_2) intermediates are more stable than Ti-OOH species.[59,60] Consequently, Ti-(η^2-O_2) may stabilize the activated forms of H_2O_2 and cause this process to be irreversible. In contrast, TBHP and CHP cannot form the Ti-(η^2-O_2) intermediate, which may make the activation of CHP and TBHP less exothermic and reversible. These findings lead to distinct rate expressions for alkene epoxidations for these different categories of peroxide oxidants (see Section 3.2).

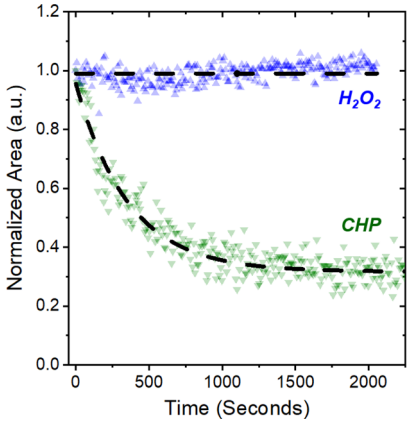

Figure 2. Areas for the LMCT bands of Ti-OOH (blue ▲) and Ti-OOcumyl (green▼) as functions of time as CH_3CN (39 mM H_2O, 313 K) flows over H_2O_2- or CHP-activated Ti-BEA-12.5, respectively. The dashed black curve for H_2O_2 is meant to guide the eye, while the curve for CHP represents an exponential decay. All areas are normalized to the initial area of the UV−vis absorbance feature (280−500 nm; Figure 1) before introducing the oxidant-free CH_3CN solution.

3.2. Elementary Steps for Alkene Epoxidations with H_2O_2 and Alkyl Hydroperoxides. Epoxidation catalysis

https://dx.doi.org/10.1021/acscatal.0c02183
ACS Catal. 2020, 10, 10169−10184

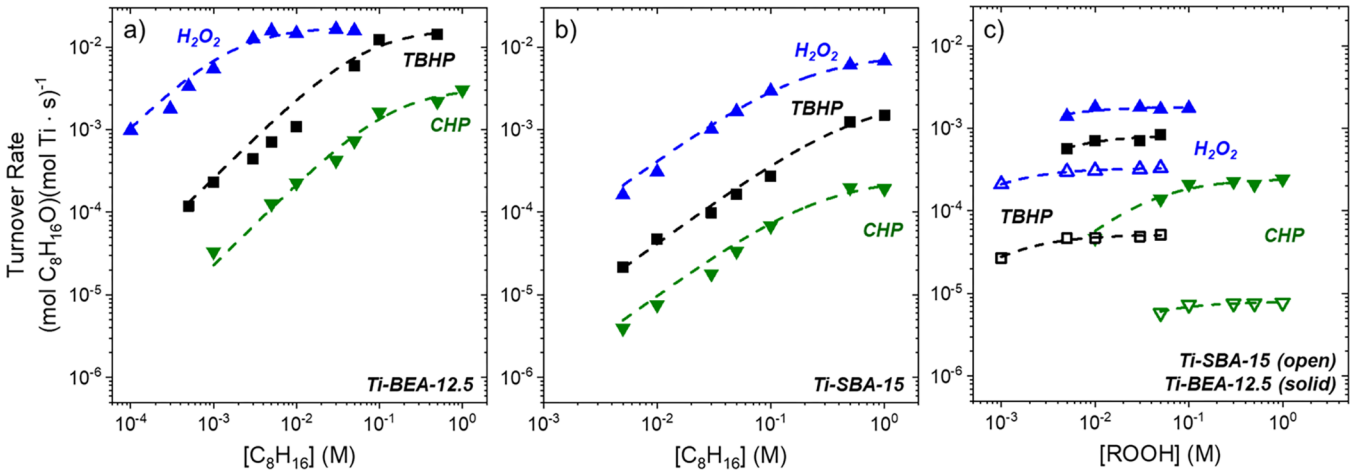

Figure 3. Turnover rates for the formation of $C_8H_{16}O$ in (a) Ti-BEA-12.5 and (b) Ti-SBA-15 as functions of $[C_8H_{16}]$ using $[H_2O_2]$ (blue ▲; 10 mM), [TBHP] (black ■; 10 mM), or [CHP] (green ▼; 0.3 M) as oxidants in CH_3CN (39 mM H_2O, 313 K). (c) Turnover rates for $C_8H_{16}O$ formation on both Ti-BEA-12.5 (closed symbols) and Ti-SBA-15 (open symbols) as functions of oxidant concentrations ([ROOH]) in CH_3CN (39 mM H_2O, 313 K), where values of $[C_8H_{16}]$ were 0.01 M for Ti-SBA-15 and 0.3, 5, and 10 mM for H_2O_2, TBHP, and CHP with Ti-BEA-12.5, respectively. The dashed lines represent fits to eqs 2a or 2b for H_2O_2 or TBHP/CHP, respectively. The rates of C_8H_{16} epoxidation with H_2O_2 over Ti-BEA-12.5 were reported initially in ref 47

Scheme 2. Proposed Catalytic Cycle for C_8H_{16} Epoxidation with Hydrogen Peroxide, *t*-butyl Hydrogen Peroxide, or Cumene Hydroperoxide over Ti-silicates[a]

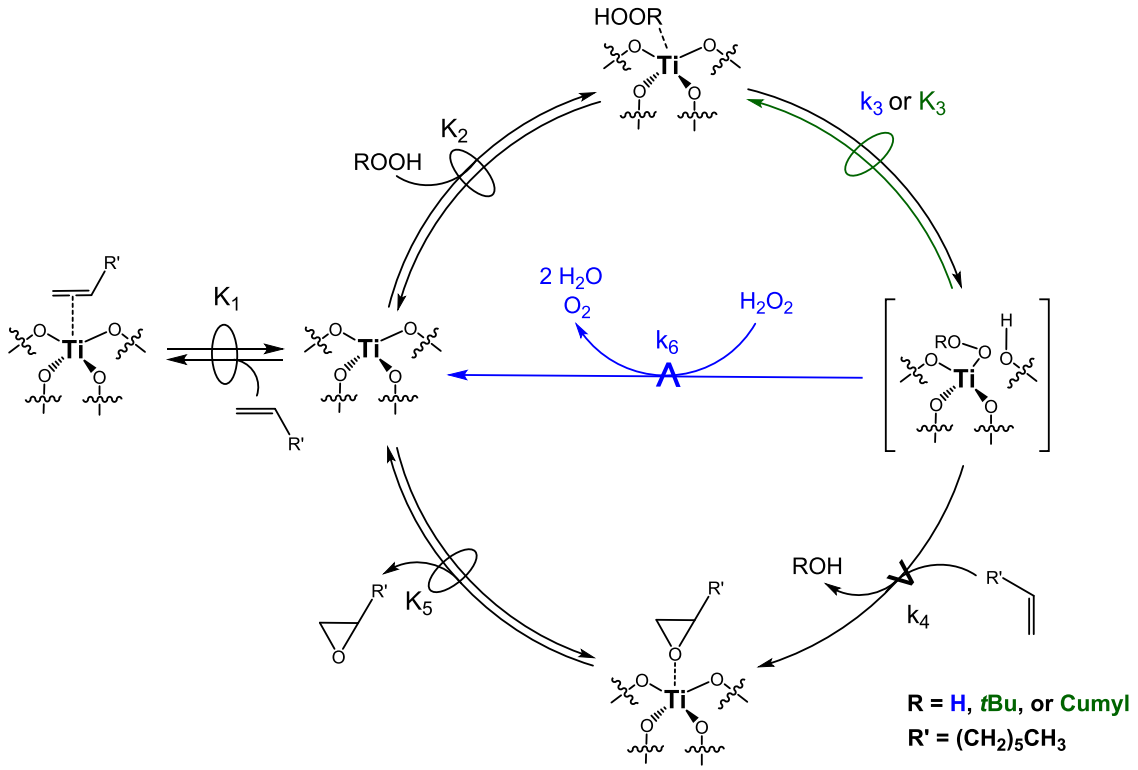

[a]The symbol ⇄ represents a quasi-equilibrated step, while → represents a kinetically relevant step. The blue arrow (and the corresponding rate constant) is unique to when H_2O_2 is used as an oxidant, while the green arrow and quasi-equilibrium in step 3 oval apply only to TBHP and CHP oxidants within this study. It should be noted that Ti atoms are likely octahedrally coordinated, where additional molecules (e.g., H_2O and CH_3CN) coordinate to the active site during catalysis. These molecules are omitted for clarity.

within zeolites and mesoporous silicates reflects the electronic contributions of Ti-OOR intermediates during O-atom transfer at epoxidation transition states, as well as interactions among activated species and their surroundings that depend on the size of the surrounding pore, the identity (and steric bulk) of the reactive species, and the solvent structures that reorganize during catalysis. A quantitative understanding of how the free energies of catalytically relevant intermediates depend on the identity of the reacting molecules and the size of the surrounding pore requires that epoxidation rates be compared at equitable

https://dx.doi.org/10.1021/acscatal.0c02183
ACS Catal. 2020, 10, 10169−10184

coverages of surface intermediates to meaningfully interpret differences in apparent activation free energies.

The rates of alkene epoxidations[47,48,58,62,63] depend on the concentrations of alkene and oxidant reactants in ways that reflect the coverages of reactive intermediates at Ti atoms and describe the series of elementary steps that lead to epoxide formation. Figure 3 shows that the turnover rates for 1-octene (C_8H_{16}) epoxidation possess the same functional dependence on the concentrations of C_8H_{16} (Figure 3a,b) and peroxide oxidants (Figure 3c) within both Ti-BEA-12.5 and Ti-SBA-15 when using H_2O_2, TBHP, or CHP. Figure S9 shows that the turnover rates for 1-octene concentration (10 mM H_2O_2) do not depend on the concentration of H_2O (8−180 mM). All reactions were performed with equal concentrations of H_2O ([H_2O]; 39 mM) to prevent differences in the amounts of intraporous H_2O from contributing to measured rates.[47,64] Differences in rates resulting from the identity of the oxidant used or pore diameters are not caused by internal mass transfer constraints, because reactions were conducted at conditions that avoid internal concentration gradients.[65] Consequently, differences in epoxidation rates reflect the changes in the electronic properties of the reactive Ti-OOR intermediates and/or configurational changes in epoxidation transition states that depend on the size of the surrounding pore.

Across all combinations of Ti-silicate and peroxide oxidants, the turnover rates for 1-octene epoxidation possess two kinetic regimes distinguished by the apparent dependence of rates on the concentrations of reactants (Figure 3). At low [C_8H_{16}], the rates increase in proportion to [C_8H_{16}] and do not depend on [ROOH], which suggests that reactive intermediates derived from the oxidant (i.e., Ti-OOR) saturate Ti active sites. The turnover rates approach constant values at higher values of [C_8H_{16}], because C_8H_{16}-derived species prevail on Ti sites as the most abundant reactive intermediates (MARIs).

Scheme 2 shows a series of elementary steps consistent with changes in turnover rates for $C_8H_{16}O$ with values of [C_8H_{16}] and [ROOH] on both Ti-BEA-12.5 and Ti-SBA-15. This catalytic cycle involves the quasi-equilibrated adsorption of C_8H_{16} (step 1) or ROOH (step 2; R = H, *t*Bu, or cumyl), and the irreversible activation of adsorbed H_2O_2 or the quasi-equilibrated activation of CHP or TBHP (step 3) to form a pool of Ti-OOR intermediates. Adsorption and activation of CHP and TBHP are presumed to be quasi-equilibrated because the rates of desorption from in situ UV−vis experiments (Figure 2, Scheme 1) are greater than the turnover rates for epoxidation. 1-Octene then adsorbs onto the pores in a quasi-equilibrated manner and undergoes kinetically relevant O-atom transfer with Ti-OOR and then forms $C_8H_{16}O$ and an equivalent of ROH (i.e., H_2O, *t*-butyl alcohol, or cumyl alcohol) (step 4). The turnover rates for ROH formation in the absence of 1-octene (i.e., TBHP and CHP decomposition) are immeasurably small ($<10^{-7}$ (mol ROH) (mol Ti·s)$^{-1}$, 10 mM TBHP or 0.3 M CHP, 313 K). In contrast, those for H_2O_2 decomposition are similar for Ti-BEA-12.5 and Ti-SBA-15 materials (∼ 2.7 (mmol H_2O_2) (mol Ti·s)$^{-1}$, 10 mM H_2O_2, 313 K) and comparable to epoxidation rates. These measurements show that a parallel pathway consumes Ti-OOH intermediates by decomposition with an additional equivalent of H_2O_2 (step 6).[62] Finally, $C_8H_{16}O$ molecules undergo quasi-equilibrated desorption (step 5) to yield the epoxide product. The rates of $C_8H_{16}O$ formation (r_E) are given by

$$r_E = k_4[C_8H_{16}][Ti - OOR] \quad (1)$$

where [Ti-OOR] is the number of reactive Ti-OOR intermediates and k_i is the rate constant for step i in Scheme 2. The use of the pseudo-steady-state hypothesis on Ti-OOH intermediates, or separately, the assumption of the quasi-equilibrated Ti-OOR (R = *t*Bu, cumyl) formation provides expressions for the number of these species, while a balance over all possible species present at Ti active sites leads to two distinct rate expressions for epoxidations. For reactions with H_2O_2, the rates take the form:

$$\frac{r_E}{[L]} = \frac{\frac{k_3k_4K_2[C_8H_{16}][H_2O_2]}{k_4[C_8H_{16}] + k_6[H_2O_2]}}{1 + K_1[C_8H_{16}] + K_2[H_2O_2] + \frac{k_3K_2[H_2O_2]}{k_4[C_8H_{16}] + k_6[H_2O_2]} + \frac{[C_8H_{16}O]}{K_5}} \quad (2a)$$

while epoxidations with TBHP and CHP are described more simply:

$$\frac{r_E}{[L]} = \frac{k_4K_2K_3[C_8H_{16}][ROOH]}{1 + K_1[C_8H_{16}] + K_2[ROOH] + K_2K_3[ROOH] + \frac{[C_8H_{16}O]}{K_5}} \quad (2b)$$

where [L] is the total number of Ti active sites and K_j is the equilibrium constant for step j. The five terms in the denominator of eqs 2a and 2b represent the number of Ti atoms covered by the molecules of CH_3CN or H_2O (i.e., the solvent), C_8H_{16}, ROOH, Ti-OOR, or $C_8H_{16}O$, respectively.

At low [C_8H_{16}], Ti-OOR intermediates form the MARI on Ti active sites, and equation 2 reduces to:

$$\frac{r_E}{[L]} = k_4[C_8H_{16}] \quad (3)$$

Equation 3 reproduces how $C_8H_{16}O$ formation rates depend on [C_8H_{16}] and [ROOH] as shown in Figure 3. Higher [C_8H_{16}] changes the MARI to become a C_8H_{16}-derived intermediate. We have previously shown that these conditions lead to $C_8H_{16}O$ as the MARI during reactions with H_2O_2.[48,58,63] These reaction conditions also give rates for epoxidation that exceed rates of H_2O_2 decomposition (i.e., $k_4[C_8H_{16}] >> k_6[H_2O_2]$, Section S3.2), which reduces eq 2a to

$$\frac{r_E}{[L]} = \frac{k_3K_2K_5[H_2O_2]}{[C_8H_{16}O]} \quad (4)$$

Alternatively, for TBHP and CHP, Ti active sites under sufficiently high [C_8H_{16}] become saturated with C_8H_{16},[66] which simplifies eq 2b

$$\frac{r_E}{[L]} = \frac{k_4K_2K_3[ROOH]}{K_1} \quad (5)$$

Equations 4 and 5 show epoxidation turnover rates that do not depend on [C_8H_{16}], which is consistent with the observations in Figure 3.

The mechanisms for epoxidations with H_2O_2, TBHP, and CHP possess many similarities, and the rate expressions simplify to identical forms when Ti-OOR species saturate active sites. The measured rates of C_8H_{16} epoxidation, however, vary by orders of magnitude between reactions conducted with different combinations of oxidants and Ti-silicates even within identical kinetic regimes (i.e., under comparable MARI). For example, the turnover rates of epoxidation with H_2O_2 on Ti-BEA-12.5 (Figure 3a, 1 mM C_8H_{16}) are 170- and 30-fold greater than those with CHP or TBHP, respectively. In contrast, epoxidation turnover rates are more similar among oxidants within Ti-SBA-15: C_8H_{16} epoxidation rates with H_2O_2 are 40- and 7-fold greater

https://dx.doi.org/10.1021/acscatal.0c02183
ACS Catal. 2020, 10, 10169−10184

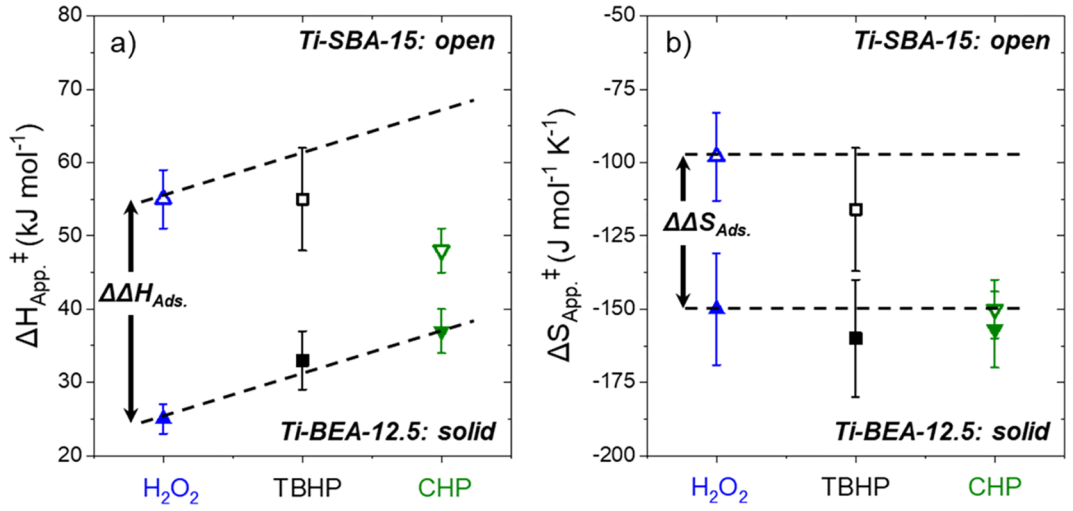

Figure 4. Values of (a) apparent activation enthalpies ($\Delta H^{\ddagger}_{App}$) and (b) apparent activation entropies ($\Delta S^{\ddagger}_{App}$) for C_8H_{16} epoxidation with H_2O_2, TBHP, and CHP over Ti-BEA-12.5 (solid symbols) and Ti-SBA-15 (open symbols) on Ti-OOR saturated active sites. For reactions with H_2O_2, differences in $\Delta H^{\ddagger}_{App}$ and $\Delta S^{\ddagger}_{App}$ between Ti-BEA-12.5 and Ti-SBA-15 represent differences in the adsorption enthalpies or entropies of C_8H_{16} into the *BEA framework, relative to SBA-15 (denoted as $\Delta\Delta H_{Ads}$ or $\Delta\Delta S_{Ads}$). The dashed lines are intended to guide the eye, and vertical offsets are set equal to the values of $\Delta\Delta H_{Ads}$ or $\Delta\Delta S_{Ads}$. Deviations from these lines for TBHP and CHP oxidants suggest differences between the conformational interactions at epoxidation transition states Ti-SBA-15 relative to Ti-BEA-12.5.

Scheme 3. Born−Haber thermochemical cycle that describes the hypothetical series of steps that form epoxidation transition states from a Ti-OOR saturated surface and a fluid-phase alkene[a]

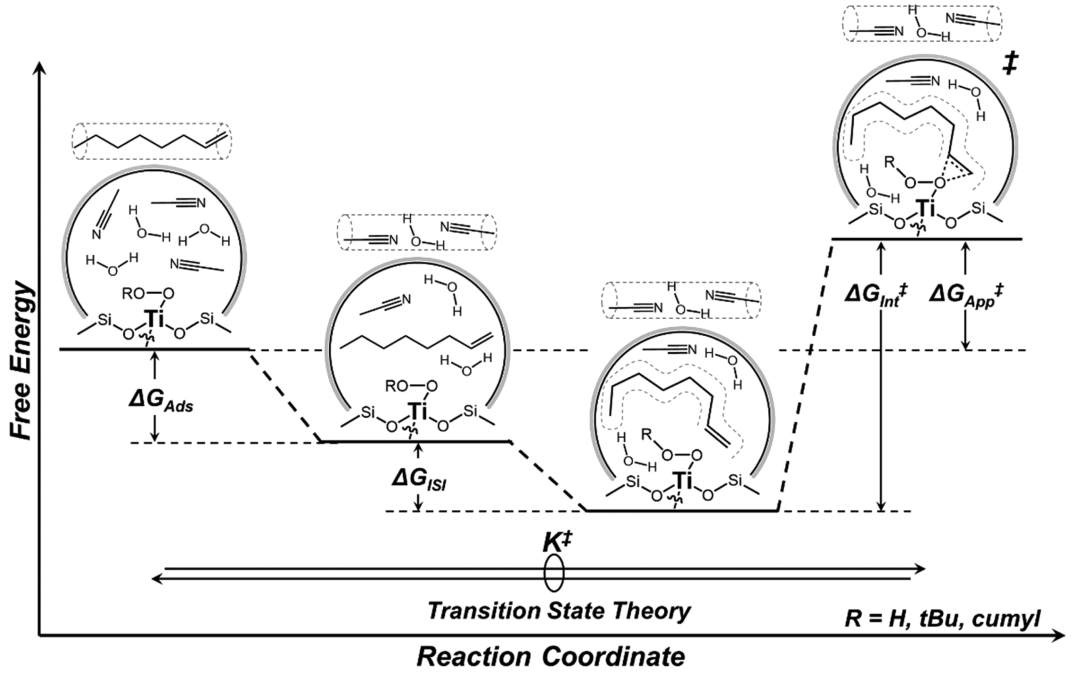

[a]Ti-OOR and fluid-phase alkene are assumed to exist in equilibrium with transition states for epoxidation. The equilibrium is described by a transition state equilibrium constant ($K^{\ddagger}$) and an apparent free energy of activation ($\Delta G^{\ddagger}_{App}$). This thermochemical sequence involves multiple steps, which include the adsorption of the alkene onto the pores (G_{Ads}), conformational arrangement of the alkene, Ti-OOR, and solvent molecules, leading to specific inner-sphere interactions (ΔG_{ISI}), and charge transfer between the Ti-OOR intermediate and the C═C to form the transition state ($\Delta G^{\ddagger}_{Int}$). The adsorption of the alkene onto the pores of the silicate displaces solvent molecules, which is depicted within a dashed cylinder. The dashed curve surrounding the alkene in states 3 and 4 represents the reorganization of the alkenes, Ti-OOR, and the surrounding solvent molecules, which lead to inner-sphere interactions among these species.

than CHP and TBHP (Figure 3b, 10 mM C_8H_{16}), respectively. Moreover, epoxidation rates are consistently 10−100 times larger within Ti-BEA-12.5 than within Ti-SBA-15, for a given oxidant. The dependence of epoxidation catalysis on the identity of the oxidant and the size of the surrounding pore likely reflects the differences in the electronic properties of the reactive Ti-OOR intermediates as well as differences in the molecular interactions among epoxidation transition states, extended silicate surfaces, and confined solvent structures.

https://dx.doi.org/10.1021/acscatal.0c02183
ACS Catal. 2020, 10, 10169−10184

3.3. Decoupling Free-Energy Contributions of Adsorption, Conformation, and Charge Transfer. Alkene epoxidations with H_2O_2, TBHP, or CHP involve reactive Ti-OOH or Ti-OOR intermediates and transition states whose stabilities depend on the electronic properties of the peroxide species in addition to interactions that depend on the size of the surrounding pore, physicochemical properties of the reacting species, and structure of the solvating molecules. Our past work shows that the electronic characteristics of Ti-OOH do not depend measurably on the topology of Ti-silicates,[47,48] which suggests that the same may hold for Ti-OO*t*Bu and Ti-OOcumyl intermediates. Intermolecular interactions between reactive species (e.g., the alkyl groups of ROOH and the alkene), however, should depend strongly on the size of the surrounding void and the proximal molecules that influence the conformations of these species. Comparisons of apparent activation free energies among distinct combinations of Ti-silicates, oxidants, and alkenes should provide insight into how these various types of interactions impact stabilities and rates.

Figure 4 shows how apparent activation enthalpies ($\Delta H^{\ddagger}_{App}$) and entropies ($\Delta S^{\ddagger}_{App}$) depend on oxidant identity within both Ti-BEA-12.5 and Ti-SBA-15. Within Ti-BEA-12.5, $\Delta H^{\ddagger}_{App}$ are the lowest with H_2O_2 and are greater by 7 and 12 kJ mol^{-1} in reactions with TBHP or CHP, respectively. The values of $\Delta S^{\ddagger}_{App}$, however, do not depend on oxidant identity within Ti-BEA-12.5, because the dominant entropy losses result from the adsorption of fluid-phase C_8H_{16} to form the epoxidation transition states. Within Ti-SBA-15, the values of $\Delta H^{\ddagger}_{App}$ are similar for epoxidations with H_2O_2 and TBHP but are 7 kJ mol^{-1} lower when CHP is used as the oxidant. The values of $\Delta S^{\ddagger}_{App}$ are 15 and 43 J mol^{-1} K^{-1} more negative than that for H_2O_2 when using TBHP or CHP, respectively. The results shown in Figure 4 clearly demonstrate that the epoxidation rates depend on the pairing of the chemical oxidant with the silicate topology but, moreover, reflect distinct ways in which the alkene and the alkyl group of the oxidant interact with their surroundings.

Transition state theory posits that the reaction rates are proportional to the number of activated complexes that exist in equilibrium with the preceding state within the catalytic cycle.[67−69] A transition state equilibrium constant, $K^{\ddagger}$, quantifies the relative number of each of these species. Under reaction conditions that result in a Ti-OOR MARI (Section 3.2; eq 3), the corresponding rate expression for epoxidation can be expressed as

$$\frac{r_E}{[L]} = \frac{k_b T}{H} e^{(-\Delta G^{\ddagger}_{App}/RT)}[C_8H_{16}] \quad (6)$$

where k_b and h are the Boltzmann and Planck constants, respectively, R is the ideal gas constant, T is the temperature in kelvin, and $\Delta G^{\ddagger}_{App}$ is the apparent free energy of activation. Here, apparent free energies of activation represent

$$\Delta G^{\ddagger}_{App} = G^{\ddagger} - G_{Ti-OOR} - G_{Alkene} \quad (7)$$

where $G^{\ddagger}$, G_{Ti-OOR}, and G_{Alkene} are the free energies of the transition states for epoxidation, the Ti-OOR intermediates, and fluid-phase alkene, respectively. Alkene adsorption into the Ti-silicate pores is quasi-equilibrated,[47,48] which conveniently allows the use of fluid-phase alkenes as the reference state to facilitate comparisons among the different combinations of catalysts and oxidants.

Born−Haber thermochemical cycles provide an approach to deconstruct the change in free energies caused by a chemical process (e.g., $\Delta G^{\ddagger}_{App}$) into a series of hypothetical intermediary steps. Scheme 3 shows such a series of steps that conveniently deconvolute interactions that contribute to the measured values of $\Delta G^{\ddagger}_{App}$. To begin, C_8H_{16} enters the voids of the Ti-silicate, displaces solvent molecules, and interacts with the surrounding pore walls, which give rise to the free energy of adsorption (ΔG_{Ads}). Next, the solvent, Ti-OOR, and C_8H_{16} undergo configurational and conformational changes that lead to inner-sphere interactions among reactive species and position the intermediates for O-atom transfer events, which subsequently form the epoxidation transition state (ΔG_{ISI}).[32,70] Finally, the epoxidation transition states form by electron exchange between the C═C and the vicinal oxygen within the Ti-OOR intermediate, which results in the intrinsic free energy of activation ($\Delta G^{\ddagger}_{Int}$). In this hypothetical cycle, the values of $\Delta G^{\ddagger}_{App}$ take the form:

$$\Delta G^{\ddagger}_{App} = \Delta G^{\ddagger}_{Int} + \Delta G_{Ads} + \Delta G_{ISI} \quad (8)$$

The ways in which $\Delta G^{\ddagger}_{Int}$, ΔG_{Ads}, and ΔG_{ISI} depend on the identity of the oxidant, size of the surrounding pore, and length of the alkene can be deconvoluted through the careful analysis of a series of kinetic experiments.

The values of $\Delta G^{\ddagger}_{Int}$ reflect the ease of transferring the proximal O-atom within Ti-OOR groups to the alkene and, therefore, should depend on the electronic properties of the alkene and Ti-OOR. Here, we examine how epoxidation rates differ between styrene and *para*-bromostyrene across the Ti-silicates and with each of the peroxide oxidants. This analysis assumes that the values of ΔG_{Ads} and ΔG_{ISI} for styrene (C_8H_8) and *p*-bromostyrene (C_8H_7Br) are indistinguishable, such that differences in the ratio of their epoxidation rates (r_{Br}/r_H) only report on differences in the electronic properties of the reactive Ti-OOR intermediates and epoxidation transition states (i.e., reflects how $\Delta G^{\ddagger}_{Int}$ values depend on oxidant and alkene identity). The ways in which r_{Br}/r_H vary with the Hammett constant (σ_{para}) is fitted using the Hammett equation in the form:

$$\log_{10}\left(\frac{r_{Br}}{r_H}\right) = \sigma_{para}\cdot\rho_{para} \sim (\Delta G^{\ddagger}_{Int,Br} - \Delta G^{\ddagger}_{Int,H})\cdot\log_{10}(e) \quad (9)$$

where r_{Br} and r_H are the epoxidation rates for (substituted) styrene epoxidation and ρ_{para} is the reaction constant, which reflects how $\Delta G^{\ddagger}_{Int}$ depends on the electronic properties of the reacting species. Figure 5 shows that the values of r_{Br}/r_H across all Ti-silicates (Ti-BEA-12.5, Ti-BEA-F, and Ti-SBA-15) are smaller when H_2O_2 is used as the oxidant (0.71 ± 0.05) and larger when using TBHP (0.86 ± 0.05) or CHP (0.90 ± 0.05), which indicates that the extent of electron exchange at the transition state differs with the oxidant used for epoxidation. Bromine functional groups are halogen-bond acceptors[71] that may form X—H bonds with H_2O localized near Ti active sites. As such, we compare rate ratios within Ti-BEA-12.5 and Ti-BEA-F (i.e., hydrophobic Ti-BEA) to determine whether the presence and proximity of H_2O to active sites affect these conclusions because Ti-BEA-F does not possess significant densities of H_2O near Ti atoms.[47] In all combinations of oxidant and silicate, the values of ρ_{para} are negative, which agrees with expectations based on the reduction of the Ti-OOR intermediate during O-atom transfer.[72] The values of ρ_{para} are largest for reactions with H_2O_2 and are smaller with TBHP or CHP because Ti-OO*t*Bu and Ti-OOcumyl intermediates are

https://dx.doi.org/10.1021/acscatal.0c02183
ACS Catal. 2020, 10, 10169−10184

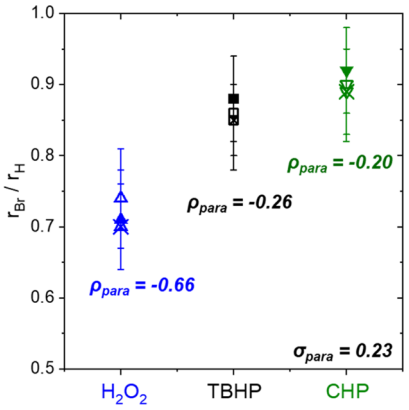

Figure 5. Ratio of epoxidation turnover rates for *p*-bromostyrene relative to styrene (r_{Br}/r_H) as a function of oxidant identity for Ti-BEA-12.5 (solid symbols), Ti-SBA-15 (open symbols), and Ti-BEA-F (symbols with an "X"). All reactions contained 10 mM alkene, 39 mM H_2O, and 10 mM H_2O_2, 10 mM TBHP, or 0.3 M CHP in CH_3CN at 313 K. The reaction constants (ρ_{para}) shown are the averaged values for all three Ti-silicates using the Hammett equation (eq 9).

less electrophilic than Ti-OOH. Consequently, these data suggest that O-atom transfer via Ti-OOH intermediates possesses a lower intrinsic energy barrier ($\Delta G^{\ddagger}_{Int}$) than reactions with Ti-OO*t*Bu or Ti-OOcumyl species.

Comparisons of ρ_{para} values across oxidants are identical within the experimental uncertainty for the three Ti-silicates examined (Ti-BEA-12.5, Ti-BEA-F, and Ti-SBA-15), which demonstrates two key points. First, these consistent trends support our assumptions that the values of ΔG_{Ads} and ΔG_{ISI} are similar for both C_8H_8 and C_8H_7Br, regardless of the size or silanol density (i.e., polarity) of the surrounding pore. Second, the uniformity of ρ_{para} values for a given oxidant suggests that the electronic properties of Ti-OOR intermediates and epoxidation transition states do not depend on the physical or chemical properties of the Ti-silicate and therefore, neither do $\Delta G^{\ddagger}_{Int}$ values.

The adsorption of alkenes from the fluid phase onto the pores of a Ti-silicate and the concomitant displacement of solvent molecules reflect the values of ΔG_{Ads} (Scheme 3) and depends strongly on the mean pore diameter and topology of the silicate.[48,62] We compare the stability of C_8H_{16} adsorbed onto Si-BEA-12.5 and SBA-15 using enthalpies of adsorption (ΔH_{Ads}), which are determined by van't Hoff analysis of C_8H_{16} uptake within CH_3CN (Section S1.3). The values of ΔH_{Ads} onto Si-BEA-12.5 and SBA-15 are equal to -85 ± 6 and -51 ± 5 kJ mol^{-1}, respectively. The difference between ΔH_{Ads} of C_8H_{16} for Si-BEA-12.5 and for SBA-15 ($\Delta\Delta H_{Ads}$; 34 kJ $\pm$ 8 mol^{-1}) resembles the difference between the values of $\Delta H^{\ddagger}_{App}$ for C_8H_{16} epoxidations with H_2O_2 for these materials ($\Delta\Delta H^{\ddagger}_{App,\ Ti-OOH} = 30 \pm 7$ kJ mol^{-1}). Consequently, the differences in epoxidation rates with H_2O_2 between Ti-BEA-12.5 and Ti-SBA-15 primarily reflect the stabilization of C_8H_{16} within the silicate pores because the electronic properties of Ti-OOH intermediates and $\Delta G^{\ddagger}_{Int}$ remain constant between these materials (vide supra). These data and interpretations agree with previous observations from our group on epoxidations over Ti-, Nb-, and Ta-silicates,[48] where the values of $\Delta\Delta H^{\ddagger}_{App}$ for styrene epoxidation with H_2O_2 among M-BEA-12.5 and mesoporous M-SiO_2 are equivalent to $\Delta\Delta H_{Ads}$ for styrene into Si-BEA-12.5 relative to SiO_2.[48] Interactions among Ti-OOH intermediates, adsorbed C_8H_{16}, and the surrounding solvent structures (i.e., ΔG_{ISI}) seem negligible, because the relatively small −OOH functions do not sense differences in the pore diameter or solvent structure within Ti-BEA-12.5 and Ti-SBA-15. Moreover, the general observation that the rates of epoxidation with H_2O_2, TBHP, or CHP (Figure 3) are greater in Ti-BEA-12.5 than in Ti-SBA-15 reflects the contributions from the stability of intrapore C_8H_{16} and the transition states that report on $\Delta\Delta H_{Ads}$.

The differences in the stability of the adsorbed alkene and the electronic properties of the Ti-OOR intermediates, however, do not explain the differences in $\Delta H^{\ddagger}_{App}$ or $\Delta S^{\ddagger}_{App}$ among the different oxidants within Ti-BEA-12.5 relative to Ti-SBA-15, which is represented by deviations from the parallel lines in Figure 4. These deviations, rather, relate to differences in the interactions among reactive species and solvent molecules that arise from molecular reorganization prior to O-atom transfer (i.e., ΔG_{ISI}, Scheme 3).

The ways that the size of the surrounding pore affects the conformation of transition states and the interactions among intraporous C_8H_{16} and Ti-OOR species can be understood by taking the difference between $\Delta G^{\ddagger}_{App}$ for reactions within Ti-SBA-15 and those in Ti-BEA-12.5:

$$\Delta\Delta G^{\ddagger}_{Pore} \equiv \Delta G^{\ddagger}_{App,Ti-SBA-15} - \Delta G^{\ddagger}_{App,Ti-BEA-12.5} = \Delta\Delta G_{Ads} + \Delta\Delta G_{ISI} \quad (10)$$

where $\Delta\Delta G_{ISI}$ represents the change in free energy associated with inner-sphere interactions among adsorbed C_8H_{16}, Ti-OOR species, and the surrounding solvent within Ti-SBA-15 relative to Ti-BEA-12.5. As described above, differences between $\Delta G^{\ddagger}_{Int}$ on these Ti-silicates are negligible.

The vertical offset in the dashed lines in Figure 4 for reactions represents the expected trends in $\Delta G^{\ddagger}_{App}$ when differences in the stability of adsorbed C_8H_{16} (i.e., $\Delta\Delta G_{Ads}$) are solely responsible for the changes in catalytic rates (i.e., if $\Delta\Delta G_{ISI}$ were negligible). The apparent deviations for the values of $\Delta H^{\ddagger}_{App}$ and $\Delta S^{\ddagger}_{App}$ of reactions with TBHP or CHP within Ti-SBA-15 strongly suggest that interactions among the −R groups, adsorbed C_8H_{16}, and the surrounding solvent depend on the size of the confining pore. Values of $\Delta\Delta H_{ISI}$ for reactions with TBHP and CHP are equal −8 and − 19 kJ mol^{-1}, respectively. Values of $\Delta\Delta S_{ISI}$ for TBHP and CHP are −15 and − 43 J mol^{-1} K^{-1}, respectively. Collectively, the mesopores of Ti-SBA-15 relative to Ti-BEA-12.5 allow for conformational changes that lower $\Delta\Delta G^{\ddagger}_{Pore}$ by 5 kJ mol^{-1} for reactions with TBHP and CHP. This decrease in free energy, afforded by the mesopores of SBA-15, shows why epoxidation rates within Ti-SBA-15 are less sensitive to oxidant identity than reactions within Ti-BEA-12.5 (Section 3.2). Further, the values of $\Delta S^{\ddagger}_{App}$ for reactions within Ti-BEA-12.5 are indistinguishable among all oxidants, which suggests that the dominant entropy loss arises from the adsorption of C_8H_{16} onto the BEA framework.

The adsorption of an alkene onto the silicate pores and subsequent interactions between reactive functions contribute to the changes in $\Delta G^{\ddagger}_{App}$. 1-Octene adsorbs exothermically onto both SBA-15 and Si-BEA-12.5; however, comparisons of $\Delta\Delta H_{ISI}$ and $\Delta\Delta S_{ISI}$ show that the interactions between reactive Ti-OO*t*Bu or Ti-OOcumyl intermediates with adsorbed C_8H_{16}, prior to the formation of transition states, do not completely offset the lower value of ΔG_{Ads} within Ti-BEA compared to Ti-SBA-15. This finding suggests that the micropores of Ti-BEA-12.5 enforce specific conformations of alkyl Ti-OOR species with C_8H_{16} during epoxidation that hinder inner-sphere interactions. In contrast, the mesopores of Ti-SBA-15 allow

https://dx.doi.org/10.1021/acscatal.0c02183
ACS Catal. 2020, 10, 10169−10184

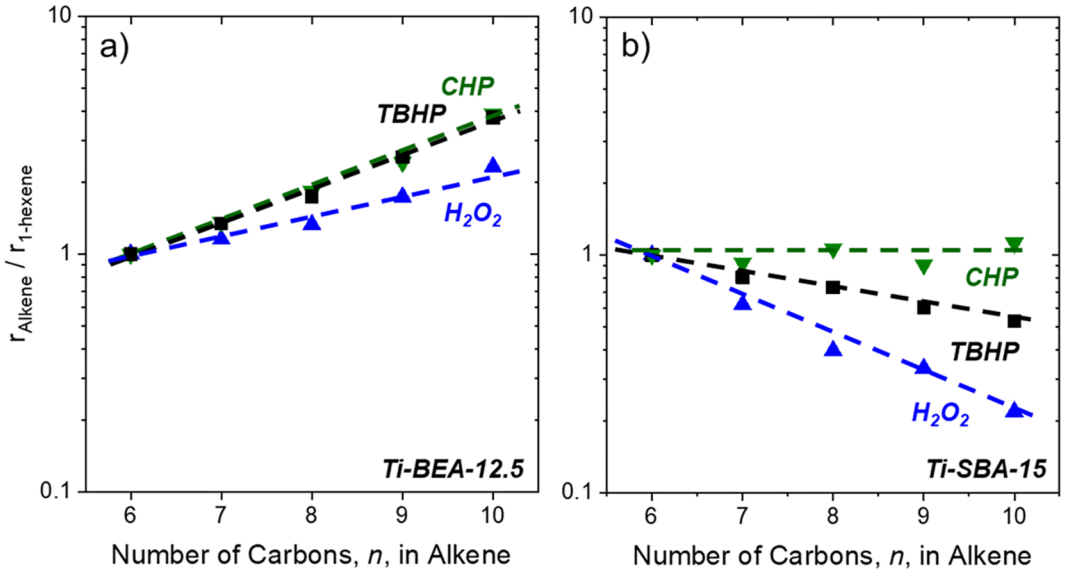

Figure 6. Ratios of epoxidation turnover rates for 1-alkenes (C_nH_{2n}, for $n = 6-10$) to those for C_6H_{12} as a function of the carbon number over (a) Ti-BEA-12.5 and (b) Ti-SBA-15 with 10 mM H_2O_2 (blue ▲), 10 mM TBHP (black ■), or 0.3 M CHP (green ▼) in CH_3CN (with 39 mM H_2O) at 313 K. In panel (a), reactions with H_2O_2, TBHP, and CHP contained 0.5, 10, or 10 mM alkene, respectively. In panel (b), all reactions contained 10 mM alkene.

the bulky alkyl Ti-OOR intermediates and C_8H_{16} molecules to access a greater range of conformations that allow for greater enthalpic stabilization (i.e., more negative $\Delta\Delta H_{ISI}$) and also increased entropic losses (i.e., more negative $\Delta\Delta S_{ISI}$).

To summarize thus far, these comparisons show that epoxidation rates depend on the oxidant identity and pore diameter in ways that reflect differences in the electronic properties of the Ti-OOR intermediates (i.e., $\Delta G^{\ddagger}_{Int}$), the stability of the intraporous alkene (i.e., ΔG_{Ads}), and interactions among reactive species and the surrounding environment (i.e., ΔG_{ISI}). Turnover rates are greatest in reactions with H_2O_2 because Ti-OOH intermediates are more electrophilic than Ti-OO*t*Bu and Ti-OOcumyl species which lowers the value of $\Delta G^{\ddagger}_{Int}$, which has the greatest impact on the measured rates. Separately, epoxidation rates are larger within Ti-BEA-12.5 than within Ti-SBA-15, for any given oxidant, because the adsorption of C_8H_{16} onto the BEA framework is more exergonic than onto SBA-15. Finally, inner-sphere interactions among reactive Ti-OOR species and specific conformations of C_8H_{16} and solvent molecules, prior to electron transfer events, lead to changes in ΔG_{ISI} that depend on the structure of the oxidant, alkene, and pore.

3.4. Effects of Steric Bulk and Pore Diameter on Transition State Stability. The ways in which the reorganization of and interactions among Ti-OOR intermediates, bound alkenes, and the surrounding solvent depend on pore diameter (i.e., ΔG_{ISI}) can be understood and quantified by systematically changing the structure of the reactants. Figure 6 shows the ratios of 1-alkene (C_6-C_{10}) epoxidation turnover rates to those for 1-hexene as functions of the chain length for reactions with H_2O_2, TBHP, and CHP in Ti-silicates. The turnover rates for 1-alkene epoxidation for all combinations of 1-alkene, oxidants, and Ti-silicates are provided in Figure S10. Within Ti-BEA-12.5, the rates of epoxidation with H_2O_2 increase by a factor of two between C_6H_{12} and $C_{10}H_{20}$ with an exponential dependence on the number of methylene units (Figure 6a). The rates of 1-alkene epoxidation with TBHP and CHP depend more strongly than H_2O_2 (i.e., increase by a factor of 4 between C_6H_{12} and $C_{10}H_{20}$; Figure 6a) on the chain length of the 1-alkene in Ti-BEA-12.5. The dependence of epoxidation rates on the 1-alkene structure for a given oxidant reflects the confluence of how both ΔG_{Ads} and ΔG_{ISI} depend on the chain length because the electronic properties of the C═C do not change significantly with the addition of a methylene group far from the double bond. If differences in ΔG_{Ads} were solely responsible for changes in the turnover rates among 1-alkenes, then epoxidations with H_2O_2, TBHP, and CHP should exhibit the same dependence on the number of methylene units. Epoxidation rates with TBHP and CHP increase with a stronger dependence on 1-alkene chain length, which suggests that the bulky Ti-OO*t*Bu and Ti-OOcumyl intermediates and surrounding solvent interact more favorably with the adsorbed alkene (i.e., stabilizing ΔG_{ISI}) than do Ti-OOH species.

Figure 6b shows that the epoxidation rates with H_2O_2 in Ti-SBA-15 decrease significantly with carbon number (by a factor of 5 between C_6H_{12} and $C_{10}H_{20}$). When TBHP is used as the oxidant, the rates of epoxidation decrease by a factor of two between C_6H_{12} and $C_{10}H_{20}$, while epoxidation rates with CHP in Ti-SBA-15 show no dependence on the chain length. In general, 1-alkene epoxidation rates decrease with the chain length in Ti-SBA-15 due to the increased entropic losses of adsorption that are not fully compensated by stabilizing dispersive interactions with the pore wall (i.e., ΔG_{Ads} becomes more positive with the chain length). Within both Ti-BEA-12.5 and Ti-SBA-15, epoxidations with H_2O_2 do not reflect significant contributions from ΔG_{ISI} (see above), which suggests that the changes in the turnover rates with the 1-alkene structure results primarily from the differences in ΔG_{Ads} within the BEA and SBA-15 pores. For both catalysts, reactions with TBHP and CHP show a more positive dependence on 1-alkene chain length than H_2O_2, which indicates that the interactions among activated oxidants, bound alkenes, and the surrounding solvent structures are stabilizing (i.e., values of ΔG_{ISI} are negative).

The free energies that describe the interactions among Ti-OOR intermediates, adsorbed alkenes, and the surrounding solvent structures before O-atom transfer (ΔG_{ISI}) can be related

https://dx.doi.org/10.1021/acscatal.0c02183
ACS Catal. 2020, 10, 10169−10184

to the quantitative measure for the steric bulk of the interacting species (e.g., the pendant alkyl groups of the oxidant and alkene), which is expressed as

$$\Delta G_{ISI} = \rho_{\ddagger}(\Omega_R + \Omega_{Alkene}) \quad (11)$$

where Ω_i is the solid angle occupied by species i (see Section S5 for given values Ω), which quantifies the steric bulk of the interacting functional groups (i.e., the −R group of Ti-OOR or the alkyl chain of the 1-alkene),[73] and $\rho_{\ddagger}$ reflects the sensitivity of ΔG_{ISI} on the steric bulk of the 1-alkene for a given combination of the oxidant and Ti-silicate. Values of ΔG_{ISI} for epoxidations with H_2O_2 are assumed to be negligible (Section 3.3), which suggests that the values of $\rho_{\ddagger,H}$ (i.e., $\rho_{\ddagger}$ for reactions with H_2O_2) are also zero. Consequently, the ways in which $\rho_{\ddagger,R}$ (R = -*t*Bu or -cumyl) depends on the pore diameter of the Ti-silicate can be determined by taking the difference in $\Delta G^{\ddagger}_{App}$ for reactions with ROOH relative to those with H_2O_2 ($\Delta\Delta G^{\ddagger}_{R-H}$)

$$\Delta\Delta G^{\ddagger}_{R-H} \equiv \Delta G^{\ddagger}_{App,ROOH} - \Delta G^{\ddagger}_{App,H_2O_2} = \Delta\Delta G^{\ddagger}_{Int,R-H} + \rho_{\ddagger,R}(\Omega_R + \Omega_{Alkene}) \quad (12)$$

where $\Delta\Delta G^{\ddagger}_{Int,R-H}$ represents the difference in the intrinsic free energies of activation for the epoxidation of a given alkene by Ti-OO*t*Bu or Ti-OOcumyl relative to Ti-OOH. By taking these differences, we remove the contributions from the ΔG_{Ads}, which depends on the structure of the 1-alkene and the topology of the silicate.

Figure 7 shows that values of $\Delta\Delta G^{\ddagger}_{R-H}$ decrease linearly with cumulative steric bulk of the alkyl function of Ti-OOR and the aliphatic tail of the 1-alkene. Within both Ti-BEA-12.5 and Ti-SBA-15, the values of $\Delta\Delta G^{\ddagger}_{Int,R-H}$ are nearly constant for a given oxidant (e.g., ∼ 15 ± 3 kJ mol^{-1} for TBHP, ∼ 23 ± 3 kJ mol^{-1} for CHP; Table 2), which confirms that these values remain independent from differences in free energies of adsorption of the alkene (ΔG_{Ads}) that would depend strongly on the size of the surrounding pore. Table 2 shows that the values of $\Delta\Delta G^{\ddagger}_{Int,R-H}$ are greater for reactions with CHP than with TBHP, which is consistent with the interpretation that Ti-OOH intermediates are more electrophilic than Ti-OO*t*Bu species, which are more electrophilic than Ti-OOcumyl intermediates. Moreover, the invariance of $\Delta\Delta G^{\ddagger}_{Int,R-H}$ for a given oxidant with pore diameter, in conjunction with Hammett analysis for substituted styrene epoxidation (Section 3.3), corroborates the finding that the electronic properties of Ti-OOR intermediates do not depend on the shape or size of the confining pore. Rather, the electronic differences among Ti-OOR depend solely on the substitution of the reactive peroxide intermediate. These interpretations regarding the effect of Ti-OOR electrophilicity on epoxidation rates (Section 3.2) agree with previous observations for alkene epoxidation[48,58] (and thiophene oxidation)[53] over early transition metals substituted into BEA-12.5 and grafted onto mesoporous SiO_2, where (ep)oxidation rates depend exponentially on the electrophilicity of M-OOH and M-(η^2-O_2) intermediates controlled by the functional Lewis acid strength of the active site (assessed by the gas-phase adsorption enthalpies of pyridine and deuterated acetonitrile).

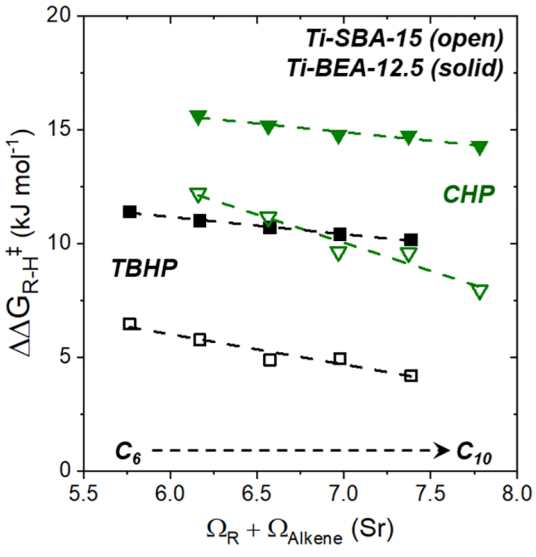

Figure 7. Differences between the apparent free energies of activation for 1-alkene epoxidation with TBHP (black ■) or CHP (green ▼) relative to 1-alkene epoxidation with H_2O_2 over Ti-BEA-12.5 (solid symbols) or Ti-SBA-15 (open symbols) as a function of the solid angle of the 1-alkene tail (e.g., *n*-butyl tail for 1-hexene). Values of $\Delta G^{\ddagger}_{App}$ were calculated from turnover rates (Figure S10) using eq 6. Dashed lines represent fits of eq 12 whose slopes and intercepts are equal to $\rho_{\ddagger,R}$ and ($\Delta G^{\ddagger}_{Int,R-H}$), respectively.

The sensitivity of the inner-sphere interactions among the reactive Ti-OOR intermediate and the aliphatic tail of the 1-alkene on pore diameter is reflected in the values of $\rho_{\ddagger,R}$. Table 2 shows that all values of $\rho_{\ddagger,R}$ are negative (Table 2), which demonstrates that these molecular interactions become more stabilizing as the steric bulk of the alkene increases. This agrees with chemical intuition, as short-ranged interactions among alkyl −R groups and aliphatic methylene chains are generally thought of as stabilizing interactions. Within Ti-BEA-12.5, the values of $\rho_{\ddagger,R}$ for TBHP and CHP are identical, which suggests that Ti-OOtBu and Ti-OOcumyl intermediates interact with the adsorbed alkenes and surrounding solvent molecules to similar extents. Values of $\rho_{\ddagger,R}$ within Ti-SBA-15, however, are significantly greater than those within Ti-BEA-12.5, which further suggests that the mesopores of SBA-15 allow for a greater number of stabilizing configurations among alkenes and Ti-OOR species that lower the free energy of the transition states. The interpretation of these data sets (Figure 7) with eq 12 to examine the inner-sphere interactions requires multiple assumptions, and the potential limitations of this approach are discussed in the Supporting Information (Section S6). Collectively, these data and interpretations show how the size of a microporous channel impacts the interactions among surface intermediates, provides a quantitative framework to interpret how the free energies of an aggregate complex depend on the size of its constituents, and helps to develop an intuition for the impact of inner-sphere interactions on catalysis at solid−liquid interfaces.

Hydroperoxide oxidants and Ti-silicate catalysts are used industrially to produce propylene oxide (PO); however, the reasons why specific combinations of oxidants, catalysts, and solvents give the greatest rates and selectivities are unclear. For example, either Ti-MFI or Ti-MWW catalysts are used with H_2O_2 in either CH_3OH or CH_3CN solvents, respectively, in variations of the hydrogen peroxide-propylene oxide (HPPO) process.[34,37] Alternatively, mesoporous Ti-SiO_2 catalysts are used for propylene epoxidations with TBHP, ethylbenzene hydroperoxide, and CHP in the propylene oxide-*tert*-butyl alcohol (PO-TBA), Shell styrene monomer-propylene oxide (SMPO), and propylene oxide-only (PO-only) processes,

https://dx.doi.org/10.1021/acscatal.0c02183
ACS Catal. 2020, 10, 10169−10184

Table 2. Sensitivities for Stabilizing Inner-Sphere Interactions among Ti-OOR Intermediates and the Aliphatic Tail of 1-Alkenes ($\rho_{\ddagger,\,R}$) and Differences in the Intrinsic Free Energies of Activation for 1-Alkene Epoxidation between TBHP or CHP and H_2O_2 ($\Delta\Delta G^{\ddagger}_{Int,\,R-H}$)[a]

sample	$\rho_{\ddagger,\,tBu}$ (kJ mol^{-1} Sr.$^{-1}$)	$\Delta\Delta G^{\ddagger}_{Int,\,tBu-H}$ (kJ mol^{-1})	$\rho_{\ddagger,\,Cumyl}$ (kJ mol^{-1} Sr.$^{-1}$)	$\Delta\Delta G^{\ddagger}_{Int,\,cumyl-H}$ (kJ mol^{-1})
Ti-BEA-12.5	−0.8 ± 0.1	15 ± 2	−0.8 ± 0.1	20 ± 2
Ti-SBA-15	−1.3 ± 0.2	14 ± 2	−2.5 ± 0.3	27 ± 2

[a]Values of $\rho_{\ddagger,\,R}$ and $\Delta\Delta G^{\ddagger}_{Int,\,R-H}$ are determined from the regression of eq 12 to the data shown in Figure 7.

respectively.[41] In general, industrial epoxidations with H_2O_2 are carried out using microporous Ti-zeolites likely because these materials selectively stabilize propylene epoxidation transition states and solvent structures that give high rates of epoxidation. In contrast, alkyl hydroperoxide oxidants in PO synthesis exclusively use mesoporous Ti-silicates. In the context of this work, the mesoporous Ti-silicates likely allow for the bulky Ti-OOR intermediates to form specific configurations with adsorbed propylene and other solvating molecules that lower the free energy of the complete activated transition state relative to within microporous Ti-zeolites and minimize differences in rates that would result from the electronic differences in Ti-OOR versus Ti-OOH intermediates. Consequently, this work partially clarifies and rationalizes why specific combinations of peroxide oxidants (i.e., H_2O_2 vs alkyl hydroperoxides) and Ti-silicates of various pore dimensions (i.e., zeolites versus mesoporous SiO_2) are chosen for an industrial process.

4. CONCLUSIONS

The turnover rates for alkene epoxidations with H_2O_2, TBHP, or CHP at Ti active sites within Ti-BEA-12.5 vary by up to a factor of 170 depending on the oxidant used. In contrast, 1-octene epoxidation rates within Ti-SBA-15 only vary by a factor of 40 among H_2O_2, TBHP, and CHP. Moreover, for any given oxidant, epoxidation rates are greater in Ti-BEA-12.5 than in Ti-SBA-15 by 10−100-fold. These differences are not due to changes in the mechanism for epoxidation, which are equivalent among all combinations of oxidants and Ti-silicates. Rather, the dependence of turnover rates on the 1-alkene chain length, oxidant identity, and zeotype pore diameter reflect differences in $\Delta G^{\ddagger}_{App}$.

Transition state theory formalisms within a Born−Haber cycle enable the deconvolution of $\Delta G^{\ddagger}_{App}$ into specific contributions from (1) the electron exchange that leads to O-atom transfer among Ti-OOR intermediates and the C=C functions ($\Delta G^{\ddagger}_{Int}$), (2) the adsorption of the alkene onto the silicate pore that occurs with the concomitant exclusion of solvent molecules (ΔG_{Ads}), and (3) the configurational and conformational changes in the adsorbed alkene, Ti-OOR intermediates, and confined solvent that lead to specific inner-sphere interactions among these species (ΔG_{ISI}). Hammett analysis of substituted-styrene epoxidation shows that the electronic properties of Ti-OOR intermediates and epoxidation transition states for a given oxidant (i.e., $\Delta G^{\ddagger}_{Int}$) do not depend on the size or the polarity of the surrounding pore. The values of $\Delta G^{\ddagger}_{Int}$, however, do show a strong dependence on the identity of the oxidant and increase as the oxidant is changed from H_2O_2 to TBHP to CHP, which rationalizes the differences in the epoxidation turnover rates among the different oxidants. Comparisons among $\Delta G^{\ddagger}_{App}$ for reactions with H_2O_2 in Ti-BEA-12.5 and Ti-SBA-15 show that the differences in epoxidation rates can be fully explained by the differences in the stability of the 1-alkene adsorbed onto the pores of the silicates (i.e., ΔG_{Ads}). Moreover, differences in ΔG_{Ads} among BEA and SBA-15 explain why, in all cases, epoxidation rates are greater within Ti-BEA-12.5 than within Ti-SBA-15. The distinct dependence of epoxidation rates on oxidant identity within the Ti-BEA-12.5 and Ti-SBA-15, however, reflects inner-sphere interactions (i.e., ΔG_{ISI}) among the Ti-OO*t*Bu and Ti-OOcumyl intermediates with the adsorbed alkene that depend on the surrounding solvent structures and the confining pore walls.

We have presented a thermodynamic model, which shows that the values of ΔG_{ISI} are proportional to a quantitative measure for the steric bulk of the reacting species (e.g., the alkyl functions of the oxidant and the alkene). The sensitivity of ΔG_{ISI} on the steric bulk of the reacting species reflects how the conformation of the aggregate complex is influenced by the size of the confining pore walls. Specifically, the mesopores of Ti-SBA-15, relative to the micropores of Ti-BEA-12.5, allow for the specific configurations of Ti-OOR intermediates and 1-alkenes that lower the free energy of the transition states and decrease the sensitivity of epoxidation rates on oxidant identity with an increasing pore diameter.

Collectively, the data and interpretations presented here show how inner-sphere interactions among reactive species can be tuned by engineering the shape and size of the surrounding pore environments and help in developing an intuition for how to conceptualize inner-sphere interactions at the solid−liquid interface.

■ ASSOCIATED CONTENT

Supporting Information

The Supporting Information is available free of charge at https://pubs.acs.org/doi/10.1021/acscatal.0c02183.

X-ray diffractograms; Tauc plots; N_2 adsorption isotherms; 1-octene uptake into *BEA and SBA-15; in situ UV−vis spectra; comparisons of rates of 1-octene epoxidation and H_2O_2 decomposition; 1-alkene epoxidation rates; steric factors; and limitations of ΔG_{ISI} (PDF)

■ AUTHOR INFORMATION

Corresponding Author

David W. Flaherty − *Department of Chemical and Biomolecular Engineering, University of Illinois at Urbana-Champaign, Urbana, Illinois 61801, United States;* orcid.org/0000-0002-0567-8481; Email: dwflhrty@illinois.edu

Authors

Daniel T. Bregante − *Department of Chemical and Biomolecular Engineering, University of Illinois at Urbana-Champaign, Urbana, Illinois 61801, United States;* orcid.org/0000-0003-2157-1286

Jun Zhi Tan − *Department of Chemical and Biomolecular Engineering, University of Illinois at Urbana-Champaign, Urbana, Illinois 61801, United States*

https://dx.doi.org/10.1021/acscatal.0c02183
ACS Catal. 2020, 10, 10169−10184

Rebecca L. Schultz − *Department of Chemical and Biomolecular Engineering, University of Illinois at Urbana-Champaign, Urbana, Illinois 61801, United States*
E. Zeynep Ayla − *Department of Chemical and Biomolecular Engineering, University of Illinois at Urbana-Champaign, Urbana, Illinois 61801, United States*
David S. Potts − *Department of Chemical and Biomolecular Engineering, University of Illinois at Urbana-Champaign, Urbana, Illinois 61801, United States;* orcid.org/0000-0001-8303-7359
Chris Torres − *Department of Chemical and Biomolecular Engineering, University of Illinois at Urbana-Champaign, Urbana, Illinois 61801, United States*

Complete contact information is available at: https://pubs.acs.org/10.1021/acscatal.0c02183

Notes

The authors declare no competing financial interest.

■ ACKNOWLEDGMENTS

We thank Ami Patel and Claudia Berdugo for technical assistance. D.T.B. was supported by the Department of Defense through the National Defense Science and Engineering Graduate (NDSEG) Fellowship Program and through a Dissertation Completion Fellowship from the University of Illinois. E.Z.A. was supported by the U.S. Army Research Office (W911NF-18-1-0100). This work was carried out, in part, in the Frederick Seitz Materials Research Laboratory. This work was supported by the Department of Energy, Office of Science, Office of Basic Energy Sciences, under Award DE-SC0020224.

■ REFERENCES

(1) Sievers, C.; Noda, Y.; Qi, L.; Albuquerque, E. M.; Rioux, R. M.; Scott, S. L. Phenomena Affecting Catalytic Reactions at Solid−Liquid Interfaces. *ACS Catal.* **2016**, *6*, 8286−8307.
(2) Bates, J. S.; Gounder, R. Influence of confining environment polarity on ethanol dehydration catalysis by Lewis acid zeolites. *J. Catal.* **2018**, *365*, 213−226.
(3) Cordon, M. J.; Harris, J. W.; Vega-Vila, J. C.; Bates, J. S.; Kaur, S.; Gupta, M.; Witzke, M. E.; Wegener, E. C.; Miller, J. T.; Flaherty, D. W.; Hibbitts, D. D.; Gounder, R. The Dominant Role of Entropy in Stabilizing Sugar Isomerization Transition States within Hydrophobic Zeolite Pores. *J. Am. Chem. Soc.* **2018**, *140*, 14244−14266.
(4) Thornburg, N. E.; Nauert, S. L.; Thompson, A. B.; Notestein, J. M. Synthesis−Structure−Function Relationships of Silica-Supported Niobium(V) Catalysts for Alkene Epoxidation with H_2O_2. *ACS Catal.* **2016**, *6*, 6124−6134.
(5) Grosso-Giordano, N. A.; Schroeder, C.; Okrut, A.; Solovyov, A.; Schöttle, C.; Chassé, W.; Marinković, N.; Koller, H.; Zones, S. I.; Katz, A. Outer-Sphere Control of Catalysis on Surfaces: A Comparative Study of Ti(IV) Single-Sites Grafted on Amorphous versus Crystalline Silicates for Alkene Epoxidation. *J. Am. Chem. Soc.* **2018**, *140*, 4956−4960.
(6) Eisenstein, O.; Crabtree, R. H. Outer sphere hydrogenation catalysis. *New J. Chem.* **2013**, *37*, 21−27.
(7) Peris, E.; Crabtree, R. H. Key factors in pincer ligand design. *Chem. Soc. Rev.* **2018**, *47*, 1959−1968.
(8) Gounder, R. Hydrophobic microporous and mesoporous oxides as Brønsted and Lewis acid catalysts for biomass conversion in liquid water. *Catal. Sci. Technol.* **2014**, *4*, 2877−2886.
(9) Gounder, R.; Davis, M. E. Beyond shape selective catalysis with zeolites: Hydrophobic void spaces in zeolites enable catalysis in liquid water. *AIChE J.* **2013**, *59*, 3349−3358.
(10) Noh, G.; Shi, Z.; Zones, S. I.; Iglesia, E. Isomerization and β-scission reactions of alkanes on bifunctional metal-acid catalysts: Consequences of confinement and diffusional constraints on reactivity and selectivity. *J. Catal.* **2018**, *368*, 389−410.
(11) Sarazen, M. L.; Iglesia, E. Stability of bound species during alkene reactions on solid acids. *Proc. Natl. Acad. Sci. U. S. A.* **2017**, *114*, E3900−E3908.
(12) Derouane, E. G. Zeolites as solid solvents. *J. Mol. Catal. A Chem.* **1998**, *134*, 29−45.
(13) Denayer, J. F.; Baron, G. V.; Martens, J. A.; Jacobs, P. A. Chromatographic Study of Adsorption of n-Alkanes on Zeolites at High Temperatures. *J. Phys. Chem. B* **1998**, *102*, 3077−3081.
(14) Bérubé, F.; Nohair, B.; Kleitz, F.; Kaliaguine, S. Controlled Postgrafting of Titanium Chelates for Improved Synthesis of Ti-SBA-15 Epoxidation Catalysts. *Chem. Mater.* **2010**, *22*, 1988−2000.
(15) Brutchey, R. L.; Ruddy, D. A.; Andersen, L. K.; Tilley, T. D. Influence of Surface Modification of Ti-SBA15 Catalysts on the Epoxidation Mechanism for Cyclohexene with Aqueous Hydrogen Peroxide. *Langmuir* **2005**, *21*, 9576−9583.
(16) Abrantes, M.; Gago, S.; Valente, A. A.; Pillinger, M.; Gonçalves, I. S.; Santos, T. M.; Rocha, J.; Romão, C. C. Incorporation of a (Cyclopentadienyl)molybdenum Oxo Complex in MCM-41 and Its Use as a Catalyst for Olefin Epoxidation. *Eur. J. Inorg. Chem.* **2004**, *2004*, 4914−4920.
(17) Bigi, F.; Piscopo, C. G.; Predieri, G.; Sartori, G.; Scotti, R.; Zanoni, R.; Maggi, R. Molybdenum-MCM-41 silica as heterogeneous catalyst for olefin epoxidation. *J. Mol. Catal. A Chem.* **2014**, *386*, 108−113.
(18) Thornburg, N. E.; Thompson, A. B.; Notestein, J. M. Periodic Trends in Highly Dispersed Groups IV and V Supported Metal Oxide Catalysts for Alkene Epoxidation with H_2O_2. *ACS Catal.* **2015**, *5*, 5077−5088.
(19) Eaton, T. R.; Boston, A. M.; Thompson, A. B.; Gray, K. A.; Notestein, J. M. Counting Active Sites on Titanium Oxide-Silica Catalysts for Hydrogen Peroxide Activation through In Situ Poisoning with Phenylphosphonic Acid. *ChemCatChem* **2014**, *6*, 3215−3222.
(20) Yoon, C. W.; Hirsekorn, K. F.; Neidig, M. L.; Yang, X.; Tilley, T. D. Mechanism of the Decomposition of Aqueous Hydrogen Peroxide over Heterogeneous TiSBA15 and TS-1 Selective Oxidation Catalysts: Insights from Spectroscopic and Density Functional Theory Studies. *ACS Catal.* **2011**, *1*, 1665−1678.
(21) Khouw, C. B.; Dartt, C. B.; Labinder, J. A.; Davis, M. E. Studies on the Catalytic Oxidation of Alkanes and Alkenes by Titanium Silicates. *J. Catal.* **1994**, *149*, 195−205.
(22) Dartt, C. B.; Davis, M. E. Characterization and catalytic activity of titanium containing SSZ-33 and aluminum-free zeolite beta. *Appl. Catal. A Gen.* **1996**, *143*, 53−73.
(23) Corma, A.; Camblor, M. A.; Esteve, P.; Martinez, A.; Perezpariente, J. Activity of Ti-Beta Catalyst for the Selective Oxidation of Alkenes and Alkanes. *J. Catal.* **1994**, *145*, 151−158.
(24) Kholdeeva, O. A. Recent developments in liquid-phase selective oxidation using environmentally benign oxidants and mesoporous metal silicates. *Catal. Sci. Technol.* **2014**, *4*, 1869−1889.
(25) Clerici, M. G.; Domine, M. E., *Oxidation Reactions Catalyzed by Transition Metal-Substituted Zeolites*. John Wiley & Sons: 2013.
(26) Bordiga, S.; Groppo, E.; Agostini, G.; van Bokhoven, J. A.; Lamberti, C. Reactivity of surface species in heterogeneous catalysts probed by in situ X-ray absorption techniques. *Chem. Rev.* **2013**, *113*, 1736−1850.
(27) Thornburg, N. E.; Notestein, J. M. Rate and Selectivity Control in Thioether and Alkene Oxidation with H_2O_2 over Phosphonate-Modified Niobium(V)-Silica Catalysts. *ChemCatChem* **2017**, *9*, 3714−3724.
(28) Ivanchikova, I. D.; Maksimchuk, N. V.; Skobelev, I. Y.; Kaichev, V. V.; Kholdeeva, O. A. Mesoporous niobium-silicates prepared by evaporation-induced self-assembly as catalysts for selective oxidations with aqueous H_2O_2. *J. Catal.* **2015**, *332*, 138−148.
(29) Morlanés, N.; Notestein, J. M. Grafted Ta−calixarenes: Tunable, selective catalysts for direct olefin epoxidation with aqueous hydrogen peroxide. *J. Catal.* **2010**, *275*, 191−201.

(30) Ruddy, D. A.; Tilley, T. D. Kinetics and Mechanism of Olefin Epoxidation with Aqueous H2O2 and a Highly Selective Surface-Modified TaSBA15 Heterogeneous Catalyst. *J. Am. Chem. Soc.* **2008**, *130*, 11088−11096.
(31) Corma, A.; Esteve, P.; Martínez, A. Solvent Effects during the Oxidation of Olefins and Alcohols with Hydrogen Peroxide on Ti-Beta Catalyst: The Influence of the Hydrophilicity-Hydrophobicity of the Zeolite. *J. Catal.* **1996**, *161*, 11−19.
(32) Clerici, M. G.; Ingallina, P. Epoxidation of Lower Olefins with Hydrogen Peroxide and Titanium Silicalite. *J. Catal.* **1993**, *140*, 71−83.
(33) Clerici, M. G. The activity of titanium silicalite-1 (TS-1): Some considerations on its origin. *Kinet. Catal.* **2015**, *56*, 450−455.
(34) Wilson, N. M.; Bregante, D. T.; Priyadarshini, P.; Flaherty, D. W. Production and Use of H_2O_2 for Atom-Efficient Functionalization of Hydrocarbons and Small Molecules. *Catalysis* **2017**, *29*, 122−212.
(35) Ratnasamy, P.; Srinivas, D.; Knözinger, H. Active Sites and Reactive Intermediates in Titanium Silicate Molecular Sieves. *Adv. Catal.* **2004**, *35*, 1−169.
(36) Moliner, M.; Corma, A. Advances in the synthesis of titanosilicates: From the medium pore TS-1 zeolite to highly-accessible ordered materials. *Microporous Mesoporous Mater.* **2014**, *189*, 31−40.
(37) Russo, V.; Tesser, R.; Santacesaria, E.; Di Serio, M. Chemical and Technical Aspects of Propene Oxide Production via Hydrogen Peroxide (HPPO Process). *Ind. Eng. Chem. Res.* **2013**, *52*, 1168−1178.
(38) LyondellBasell's $2.4bn PO/TBA project driven by technology and feedstocks. https://www.icis.com/explore/resources/news/2017/07/26/10127843/lyondellbasell-s-2-4bn-po-tba-project-driven-by-technology-and-feedstocks/(accessed March 2nd, 2020).
(39) Weissermel, K.; Arpe, H.-J., *Industrial Organic Chemistry*. Fourth ed.; Wiley-VCH: 2003.
(40) Mimoun, H. Do metal peroxides as homolytic and heterolytic oxidative reagents. Mechanism of the halcon epoxidation process. *Catal. Today* **1987**, *1*, 281−295.
(41) Development of New Propylene Oxide Process. https://www.sumitomo-chem.co.jp/english/rd/report/files/docs/20060100_ely.pdf (accessed May 7th, 2020)
(42) Xia, Q. H.; Chen, X.; Tatsumi, T. Epoxidation of cyclic alkenes with hydrogen peroxide and tert-butyl hydroperoxide on Na-containing Ti-Beta zeolites. *J. Mol. Catal. A Chem.* **2001**, *176*, 179−193.
(43) Fraile, J. M.; García, J. I.; Mayoral, J. A.; Vispe, E.; Brown, D. R.; Naderi, M. Is MCM-41 really advantageous over amorphous silica? The case of grafted titanium epoxidation catalysts. *Chem. Commun.* **2001**, 1510−1511.
(44) Sanz, R.; Serrano, D. P.; Pizarro, P.; Moreno, I. Hierarchical TS-1 zeolite synthesized from SiO_2-TiO_2 xerogels imprinted with silanized protozeolitic units. *Chem. Eng. J.* **2011**, *171*, 1428−1438.
(45) Blasco, T.; Camblor, M. A.; Corma, A.; Esteve, P.; Guil, J. M.; Martínez, A.; Perdigón-Melón, J. A.; Valencia, S. Direct synthesis and characterization of hydrophobic aluminum-free Ti-beta zeolite. *J. Phys. Chem. B* **1998**, *102*, 75−88.
(46) Chorkendorff, I.; Niemantsverdriet, J. W. H., *Concepts of Modern Catalysis and Kinetics*. 2nd ed.; Wiley-VCH Verlag Gmbh & Co.: Weinheim, 2007.
(47) Bregante, D. T.; Johnson, A. M.; Patel, A. Y.; Ayla, E. Z.; Cordon, M. J.; Bukowski, B. C.; Greeley, J.; Gounder, R.; Flaherty, D. W. Cooperative Effects between Hydrophilic Pores and Solvents: Catalytic Consequences of Hydrogen Bonding on Alkene Epoxidation in Zeolites. *J. Am. Chem. Soc.* **2019**, *141*, 7302−7319.
(48) Bregante, D. T.; Thornburg, N. E.; Notestein, J. M.; Flaherty, D. W. Consequences of Confinement for Alkene Epoxidation with Hydrogen Peroxide on Highly Dispersed Group 4 and 5 Metal Oxide Catalysts. *ACS Catal.* **2018**, *8*, 2995−3010.
(49) Ruddy, D. A.; Brutchey, R. L.; Tilley, T. D. The Influence of Surface Modification on the Epoxidation Selectivity and Mechanism of TiSBA15 and TaSBA15 Catalysts with Aqueous Hydrogen Peroxide. *Top. Catal.* **2008**, *48*, 99−106.
(50) Bonino, F.; Damin, A.; Ricchiardi, G.; Ricci, M.; Spanò, G.; D'Aloisio, R.; Zecchina, A.; Lamberti, C.; Prestipino, C.; Bordiga, S. Ti-Peroxo Species in the Ts-1/H2O2/H2O System. *J. Phys. Chem. B* **2004**, *108*, 3573−3583.
(51) Bordiga, S.; Damin, A.; Bonino, F.; Ricchiardi, G.; Lamberti, C.; Zecchina, A. The Structure of the Peroxo Species in the TS-1 Catalyst as Investigated by Resonant Raman Spectroscopy. *Angew. Chem. Int. Ed. Engl.* **2002**, *41*, 4734−4737.
(52) Gleeson, D.; Sankar, G.; Catlow, C. R. A.; Meurig, T. J.; Spanó, G.; Bordiga, S.; Zecchina, A.; Lamberti, C. The architecture of catalytically active centers in titanosilicate (TS-1) and related selective-oxidation catalysts. *Phys. Chem. Chem. Phys.* **2000**, *2*, 4812−4817.
(53) Bregante, D. T.; Patel, A. Y.; Johnson, A. M.; Flaherty, D. W. Catalytic Thiophene Oxidation by Groups 4 and 5 Framework-Substituted Zeolites with Hydrogen Peroxide: Mechanistic and Spectroscopic Evidence for the Effects of Metal Lewis Acidity and Solvent Lewis Basicity. *J. Catal.* **2018**, *364*, 415−425.
(54) Hydroperoxide, 1-methyl-1-phenylethyl. https://webbook.nist.gov/cgi/cbook.cgi?Source=1969FIH%2F141&Mask=400 (accessed February 25th, 2020).
(55) Barker, C. M.; Gleeson, D.; Kaltsoyannis, N.; Catlow, C. R. A.; Sankar, G.; Thomas, J. M. On the structure and coordination of the oxygen-donating species in Ti↑MCM-41/TBHP oxidation catalysts: a density functional theory and EXAFS study. *Phys. Chem. Chem. Phys.* **2002**, *4*, 1228−1240.
(56) Sankar, G.; Thomas, J. M.; Catlow, C. R. A.; Barker, C. M.; Gleeson, D.; Kaltsoyannis, N. The Three-Dimensional Structure of the Titanium-Centered Active Site during Steady-State Catalytic Epoxidation of Alkenes. *J. Phys. Chem. B* **2001**, *105*, 9028−9030.
(57) Kwon, S.; Schweitzer, N. M.; Park, S.; Stair, P. C.; Snurr, R. Q. A kinetic study of vapor-phase cyclohexene epoxidation by H_2O_2 over mesoporous TS-1. *J. Catal.* **2015**, *326*, 107−115.
(58) Bregante, D. T.; Flaherty, D. W. Periodic Trends in Olefin Epoxidation over Group IV and V Framework Substituted Zeolite Catalysts: A Kinetic and Spectroscopic Study. *J. Am. Chem. Soc.* **2017**, *139*, 6888−6898.
(59) Zhang, T.; Mazaud, L.; Chamoreau, L.-M.; Paris, C.; Proust, A.; Guillemot, G. Unveiling the Active Surface Sites in Heterogeneous Titanium-Based Silicalite Epoxidation Catalysts: Input of Silanol-Functionalized Polyoxotungstates as Soluble Analogues. *ACS Catal.* **2018**, *8*, 2330−2342.
(60) Maksimchuk, N. V.; Ivanchikova, I. D.; Maksimov, G. M.; Eltsov, I. V.; Evtushok, V. Y.; Kholdeeva, O. A.; Lebbie, D.; Errington, R. J.; Solé-Daura, A.; Poblet, J. M.; Carbó, J. J. Why Does Nb(V) Show Higher Heterolytic Pathway Selectivity Than Ti(IV) in Epoxidation with H2O2? Answers from Model Studies on Nb- and Ti-Substituted Lindqvist Tungstates. *ACS Catal.* **2019**, *9*, 6262−6275.
(61) Jiménez-Lozano, P.; Ivanchikova, I. D.; Kholdeeva, O. A.; Poblet, J. M.; Carbó, J. J. Alkene oxidation by Ti-containing polyoxometalates. Unambiguous characterization of the role of the protonation state. *Chem. Commun.* **2012**, *48*, 9266−9268.
(62) Bregante, D. T.; Tan, J. Z.; Sutrisno, A.; Flaherty, D. W. Heteroatom substituted zeolite FAU with ultralow Al contents for liquid-phase oxidation catalysis. *Catal. Sci. Technol.* **2020**, *10*, 635−647.
(63) Bregante, D. T.; Priyadarshini, P.; Flaherty, D. W. Kinetic and spectroscopic evidence for reaction pathways and intermediates for olefin epoxidation on Nb in * BEA. *J. Catal.* **2017**, *348*, 75−89.
(64) Bregante, D. T.; Flaherty, D. W. Impact of Specific Interactions Among Reactive Surface Intermediates and Confined Water on Epoxidation Catalysis and Adsorption in Lewis Acid Zeolites. *ACS Catal.* **2019**, *9*, 10951−10962.
(65) Madon, R. J.; Boudart, M. Experimental Criterion for the Absence of Artifacts in the Measurement of Rates of Heterogeneous Catalytic Reactions. *Ind. Eng. Chem. Fundam.* **1982**, *21*, 438−447.
(66) At high $[C_8H_{16}]$ in reactions with TBHP and CHP, $C_8H_{16}O$ is not assumed to be the MARI because this would lead to a first-order dependence on $[C_8H_{16}]$, which is not what is observed in Figure 3.
(67) Flaherty, D. W.; Iglesia, E. Transition-state enthalpy and entropy effects on reactivity and selectivity in hydrogenolysis of n-alkanes. *J. Am. Chem. Soc.* **2013**, *135*, 18586−18599.

(68) Bhan, A.; Gounder, R.; Macht, J.; Iglesia, E. Entropy considerations in monomolecular cracking of alkanes on acidic zeolites. *J. Catal.* **2008**, *253*, 221−224.
(69) Wilson, N. M.; Schröder, J.; Priyadarshini, P.; Bregante, D. T.; Kunz, S.; Flaherty, D. W. Direct synthesis of H_2O_2 on PdZn nanoparticles: The impact of electronic modifications and heterogeneity of active sites. *J. Catal.* **2018**, *368*, 261−274.
(70) Stare, J.; Henson, N. J.; Eckert, J. Mechanistic Aspects of Propene Epoxidation by Hydrogen Peroxide. Catalytic Role of Water Molecules, External Electric Field, and Zeolite Framework of TS-1. *J. Chem. Inf. Model.* **2009**, *49*, 833−846.
(71) Cavallo, G.; Metrangolo, P.; Milani, R.; Pilati, T.; Priimagi, A.; Resnati, G.; Terraneo, G. The Halogen Bond. *Chem. Rev.* **2016**, *116*, 2478−2601.
(72) Anslyn, E. V.; Dougherty, D. A., *Modern Physical Organic Chemistry*. University Science: 2005.
(73) White, D.; Coville, N. J. Quantification of Steric Effects in Organometallic Chemistry. *Adv. Organomet. Chem.* **1994**, *36*, 95−158.

https://dx.doi.org/10.1021/acscatal.0c02183
ACS Catal. 2020, 10, 10169−10184